Animal Intermittent Locomotion: A Null Model for the Probability of Moving Forward in Bounded Space

Kim Christensen[1,2], Luca Cocconi[1,2,3], and Ana B. Sendova-Franks[4]

[1]Blackett Laboratory, Imperial College London, London SW7 2AZ, UK
[2]Center for Complexity Science, Imperial College London, London SW7 2AZ, UK
[3]Theoretical Physics of Biology Laboratory, The Francis Crick Institute, London NW1 1AT, UK
[4]School of Biological Sciences, University of Bristol, 24 Tyndall Avenue, Bristol BS8 1TQ, UK

November 23, 2020

Keywords: Movement within bounded space, geometry of bounded space, persistence in movement between stops in intermittent locomotion, random walk, decision-making

Abstract

We present a null model to be compared with biological data to test for intrinsic persistence in movement between stops during intermittent locomotion in bounded space with different geometries and boundary conditions. We describe spatio-temporal properties of the sequence of stopping points $\mathbf{r}_1, \mathbf{r}_2, \mathbf{r}_3, ...$ visited by a Random Walker within a bounded space. The path between stopping points is not considered, only the displacement. Since there are no intrinsic correlations in the displacements between stopping points, there is no intrinsic persistence in the movement between them. Hence, this represents a null-model against which to compare empirical data for directional persistence in the movement between stopping points when there is external bias due to the bounded space. This comparison is a necessary first step in testing hypotheses about the function of the stops that punctuate intermittent locomotion in diverse organisms. We investigate the probability of forward movement, defined as a deviation of less than 90° between two successive displacement vectors, as a function of the ratio between the largest displacement between stops that could be performed by the random walker and the system size, $\alpha = \Delta\ell/L_{\max}$. As expected, the probability of forward movement is $1/2$ when $\alpha \to 0$. However, when α is finite, this probability is less than $1/2$ with a minimum value when $\alpha = 1$. For certain boundary conditions, the minimum value is between $1/3$ and $1/4$ in 1D while it can be even lower in 2D. The probability of forward movement in 1D is calculated exactly for all values $0 < \alpha \leq 1$ for several boundary conditions. Analytical calculations for the probability of forward movement are performed in 2D for circular and square bounded regions with one boundary condition. Numerical results for all values $0 < \alpha \leq 1$ are presented for several boundary conditions. The cases of rectangle and ellipse are also considered and an approximate model of the dependence of the forward movement probability on the aspect ratio is provided. Finally, some practical points are presented on how these results can be utilised in the empirical analysis of animal movement in two-dimensional bounded space.

1 Introduction

The movement of animals contains information about how they operate. The idea of movement as the communication of intention from the brain to the environment is a new point of convergence between cognitive neuroscience and the systems approach to neurophysiology [1]. Tinbergen, one of the fathers of the study of animal behaviour as a science, famously said that all behaviour is movement [2]. Traditionally, locomotion, the type of movement that is about displacement in space, has been the focus of ecologists interested in dispersal, foraging and migration [3, 4, 5, 6]. More recently, the paradigm of movement ecology has striven to unify the analysis of the sequential positions of animals with information about their physiological and behavioural state and the influence of external factors [7]. This approach has benefitted from the inclusion of the intermittency that characterizes locomotion and behaviour in general [8, 9, 10, 11]. Animals stop and go

or, as O'Brien *et al.* [8] put it, animals have a saltatory pattern of movement. The pauses punctuating locomotion could allow resting, perception [9] or making decisions about the next move [13, 14]. As such they could also represent opportunities for changing the direction of movement [11].

The Simple Random Walk (SRW) model paradigm is based on the movement trajectory and does not include behavioural intermittence [15] while the more recent Multiple Random Walk (MRW) model paradigm focuses on the identification of behavioural modes from the movement trajectory arising in response to external factors [11]. The very recent Intermittent Random Walk (IRW) paradigm specifically focuses on incorporating behavioural intermittence [12], which is assumed to have predominantly an internal origin [11, 16, 17]. A fundamental question in empirical studies of intermittent movement is whether it displays forward persistence [18, 19, 20] after a pause. This can be tested with established methods such as the mean squared displacement [21], the Marsh-Jones statistic [22], net displacement against path length [23], or the distribution of the turning angle, among others [23, 24]. These methods assume the environment is unrestricted and the movement persistence is intrinsic to the organism. Here, by contrast, our null model allows tests for persistence in the presence of external bias [25]. The question this null model addresses is: If the studied individual has no intrinsic persistence, what would be its probability of moving forward given the external bias resulting from the boundedness and geometry of the space? Such a null model is crucial for testing whether animals studied in bounded environments display directional persistence in their movement between stops that is intrinsic to them and cannot be explained purely by environmental constraints.

The effect of bounded space on random-walk models has been considered in, for example, the context of worker sorting inside ant nests [26] and the spatial distribution of cockroaches [27]. A recent study explored the efficiency of different trap shapes in catching ground-dwelling arthropods modelled as random walkers [28]. However, to the best of our knowledge, the present study is the first to address the effect of bounded space and its geometry on the expected probability of moving forward.

We focus on the sequence of stopping positions $\mathbf{r}_1, \mathbf{r}_2, \mathbf{r}_3, \ldots$ and the associated displacement vectors between the stops. The simplest question one might ask is whether, after a stop at say $\mathbf{r}_2$, an animal moves forward or backward relative to the displacement vector, $\mathbf{r}_2 - \mathbf{r}_1$, allowing us to test for the presence of persistence in displacement vectors in between stops. The null model against which we can compare experimental data should be a model without any bias, that is, a model that produces displacement stopping points without any correlation between them. Naively, according to our definition of forward movement above, one might expect the probability of forward movement after a pause under this null model to equal $\frac{1}{2}$. This is indeed the case in situations where animals move

within unbounded space. However, many animals move within ranges or home territories [29, 30] and spatial segregation of movement is a common characteristic of populations [31]. Furthermore, locomotion characteristics are among the main measurements of exploratory behaviour across animal species and these are often recorded within bounded space [32, 33, 34]. If the animal moves in a random direction and with a random displacement after a pause but the movement is in a bounded space and the animal happens to move towards the boundary in one direction, there will be less of the bounded area in that direction. Therefore, the probability of moving forward after the next pause would in fact be less than $\frac{1}{2}$.

2 Paper layout

We begin with an outline of our theoretical methodology, which involves analytical calculations and Monte Carlo simulations (section 3). Then, before we consider the expected probability for moving forward under the null model with randomly placed stopping positions in two dimensions, we introduce the mathematically simpler situation in one dimension. Indeed, the insight from this simpler study qualitatively transfers to the more biologically relevant situation in 2D and thereby develops our intuitive understanding of the main conclusions.

In the following, we focus on a model with impermeable boundary and a "no-go" boundary condition where steps extending beyond the bounded space are rejected, but we also investigate the effect of other boundary conditions [35] in the appendix. The displacements between stops are sampled from a uniform distribution within circle of radius $\Delta\ell$. We will show that the dimensionless ratio, $\alpha = \Delta\ell/L_{\max}$, where $\Delta\ell = \max|\mathbf{r}_{j+1} - \mathbf{r}_j|$ is the magnitude of the maximum displacement and $L_{\max}$ the maximum linear dimension of the bounded space, controls the probability of moving forward. In section 4, we demonstrate that the probability of moving forward in a one-dimensional interval $p_{1\mathrm{D}}(\alpha) = \frac{1}{3}$ when $\alpha = \Delta\ell/L_{\max} = 1$. Likewise, we show analytically that the probability of moving forward in a one-dimensional interval $p_{1\mathrm{D}}(\alpha) = \frac{1}{2}$ when $\alpha \to 0$. We present numerical results for $0 < \alpha \leq 1$ that reveal the probability $p_{1\mathrm{D}}(\alpha)$ crosses over from $\frac{1}{3}$ to $\frac{1}{2}$ when α decreases from 1 towards 0. The numerical results are consistent with exact analytic results of the crossover probabilities derived in appendix A.

In section 5, we consider the $2D$ regions of the unit circle and the unit square for the "no-go" boundary condition. We derive analytic results for the unit circle and square when $\alpha = 1$. For the circle, we derive the analytic result for $p_{\bigcirc}(\alpha)$ in the whole range $0 < \alpha \leq 1$ and we present numerical results for the square $p_{\square}(\alpha)$. The results reveal a crossover from the analytically determined $p_{\bigcirc}(\alpha) = 0.23990508\ldots$ and $p_{\square}(\alpha) = 0.2417354\ldots$, respectively, to $p_{\bigcirc}(\alpha) = p_{\square}(\alpha) = \frac{1}{2}$ when α decreases from 1 towards 0. We demonstrate that these results hold for any circle and square, independently of the associated $L_{\max}$, assuming α is fixed. In this section we also consider the cases of the unit ellipse and the

unit rectangle in the whole range $0 < \alpha \leq 1$. With an aspect ratio of one, we find the results mentioned above. In the limit of the aspect ratio going to zero, the probability of forward movement tends to the one-dimensional result of $\frac{1}{3}$ as expected.

In section 6, we present practical advice on how to compare empirical results with the expected values based on our null model with randomly placed stopping positions in two dimensions. We provide a step-by-step procedure for such comparisons in Appendix E. Our aim is to help researchers test whether their study organism is more likely or less likely than expected to move forwards between successive stop locations within a rectangular or elliptical bounded region. Such a test reveals whether the studied organism has directional persistence in its movement between stops.

Finally, we summarise our findings and conclusions and comment on future research.

3 Methodology

In this paper, we will focus on the "no-go" boundary condition, that is, steps that fall outside the bounded region are rejected. There are other choices of boundary conditions, e.g. the "stop-go" boundary condition where such steps are terminated on the boundary or "reflective" boundary conditions where the portion of the step that would fall outside the boundary is reflected back into the region [35]. The "no-go" boundary condition is natural for animals that have habituated to their environment but for completeness, we consider the effect of the two other boundary conditions in the appendix.

3.1 Analytical calculations

Given a bounded region $\mathcal{R}$, the probability of moving forward $p_{\mathcal{R}}(\alpha)$ when the stopping positions are distributed uniformly at random in space, $\alpha = 1$, is calculated by considering a triplet of points $\mathbf{r}_1, \mathbf{r}_2$ and $\mathbf{r}_3$. Choose the position of the first two points at random within the bounded region $\mathcal{R}$ and consider the displacement vector $\mathbf{r}_{12} = \mathbf{r}_2 - \mathbf{r}_1$. This displacement vector would uniquely determine the fraction $p_{\mathcal{R}}(\mathbf{r}_1, \mathbf{r}_2)$ of the region $\mathcal{R}$ where the point $\mathbf{r}_3$ can be placed for forward movement, see hatched area in Fig. 1. If we can find an analytic expression for $p_{\mathcal{R}}(\mathbf{r}_1, \mathbf{r}_2)$, then, for $\alpha = 1$, the probability of moving forward is found by averaging over all possible positions of the first two points within the region $\mathcal{R}$.

Given $\alpha = \Delta\ell / L_{\max} < 1$ and the first stopping point $\mathbf{r}_1$, draw a circle centered at $\mathbf{r}_1$ with radius $\Delta\ell$. For the "no-go" boundary condition, the next stopping point $\mathbf{r}_2$ is chosen randomly in the area confined within this circle and the region $\mathcal{R}$. The stopping point $\mathbf{r}_3$ is found in a similar way: draw a circle centered at $\mathbf{r}_2$ and then choose a point randomly within the area given by the intersection of this circle and the region $\mathcal{R}$.

3.2 Monte Carlo simulations

For details of the Monte Carlo simulations, please see Appendix D.

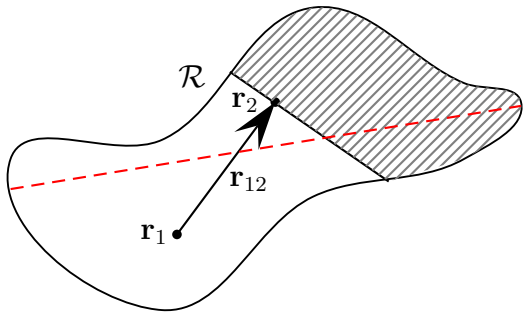

Figure 1: A bounded region $\mathcal{R}$. The dashed red line indicates the maximum linear dimension of the region, $L_{\max}$. The displacement vector $\mathbf{r}_{12} = \mathbf{r}_2 - \mathbf{r}_1$ from the stopping positions $\mathbf{r}_1$ to $\mathbf{r}_2$ defines the fraction of the region $p_{\mathcal{R}}(\mathbf{r}_1, \mathbf{r}_2)$ (hatched area) where the move from $\mathbf{r}_2$ to $\mathbf{r}_3$ would be forward relatively to $\mathbf{r}_{12}$.

4 One-dimensional case

In this section, we will give analytical results for the "no-go" boundary condition but we also comment on other boundary conditions and give analytical results for those in the appendix.

4.1 Interval with $\alpha = 1$

Consider a one-dimensional interval $0 \leq x \leq 1$. We will show that the probability of going forward in a sequence of randomly chosen stopping positions equals $\frac{1}{3}$ for the "no-go" boundary condition.

Consider choosing three points x_1, x_2 and x_3 at random. Such a movement is forward going only if $x_3 > x_2 > x_1$ (i.e., if x_2 is to the right of x_1, x_3 must be to the right of x_2) or $x_3 < x_2 < x_1$ (i.e., if x_2 is to the left of x_1, x_3 must be to the left of x_2), see Fig. 2. We will use a combinatorial argument: Consider the three randomly chosen points x_1, x_2

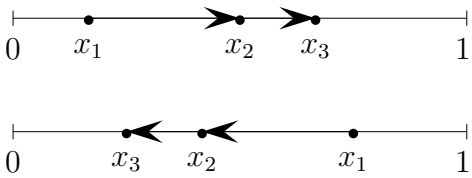

Figure 2: An interval in 1D is a straight line. Let x_1, x_2, and x_3 be three consecutive stopping points. Shown are the two cases where forward movement is taking place: $x_3 > x_2 > x_1$ or $x_3 < x_2 < x_1$.

and x_3 and place them in ascending order

$$x_1 > x_2 > x_3 \quad \text{or} \quad x_3 > x_2 > x_1, \tag{1a}$$
$$x_1 > x_3 > x_2 \quad \text{or} \quad x_3 > x_1 > x_2, \tag{1b}$$
$$x_2 > x_3 > x_1 \quad \text{or} \quad x_2 > x_1 > x_3. \tag{1c}$$

There are six possible combinations. Only the two first of these combinations shown in Eq.(1a) are categorized as forward movement, see Fig. 2. Because all combinations are equally probable, with probability $\frac{1}{6}$, that yields a probability $p_{1\mathrm{D}}(\alpha) = \frac{1}{3}$ of going forward for $\alpha = 1$. This result is independent on the length of the interval as long as $\alpha = 1$. One can reach the same conclusion by mathematical analysis, see Appendix A.1.1. The above calculation assumes that the stopping positions are chosen at random, that is, that the stopping positions have no restrictions except that they cannot be beyond the boundaries of the space, that is, the "no-go" boundary condition. This is the limiting case $\alpha = 1$.

4.2 Interval with $0 < \alpha \leq 1$

If we assume that the displacement between stopping positions is randomly chosen in the interval $[-\Delta\ell, \Delta\ell]$, again under the restriction that one cannot go beyond the space boundary, we can perform numerical simulations to estimate the probability of moving forward. Indeed, we can even find analytic results for all values of $0 < \alpha = \Delta\ell/L_{max} \leq 1$. The derivation of these exact probabilities being less intuitive than simple combinatorics, we will only present the final results here and leave the details for Appendix A.1.3.

Following the algorithm described in Appendix D with $M = 5 \cdot 10^6$ and $N = 1000$ we perform Monte Carlo simulations with a variable dimensionless ratio α. When $\alpha = 1$, then the next stopping point is chosen at random within the bounded region because all points are accessible as the maximum displacement $\Delta\ell = L_{\max}$. The numerical results are consistent with the analytic result of $p_{1\mathrm{D}}(\alpha) = \frac{1}{3}$ for $\alpha = 1$, see Fig. 3. However, when $\alpha < 1$, consecutive stopping positions have to be within distance $\Delta\ell < L_{\max}$. If $\alpha \to 0$, then the bounded region plays no role and we can show analytically that $p_{1\mathrm{D}}(\alpha) = \frac{1}{2}$, see Appendix A.1.2. Indeed, the numerical estimates from the Monte Carlo simulations display a crossover from $p_{1\mathrm{D}}(\alpha) = \frac{1}{3}$ when $\alpha = 1$ to $p_{1\mathrm{D}}(\alpha) = \frac{1}{2}$ when $\alpha \to 0$, see Fig. 3.

The analytical solution for $p_{1\mathrm{D}}(\alpha)$ as a function of $\alpha = \Delta\ell/L_{max}$ has the form

$$p_{1\mathrm{D}}(\alpha) = \begin{cases} \dfrac{1 + 2\alpha(1 - 2\log(2))}{2 - \alpha} & \text{for } \alpha \leq 1/2, \\ \dfrac{4}{2 - \alpha}\left(1 + \alpha\log\alpha - \dfrac{6\alpha^2 + 4\alpha^3 + 1}{12\alpha}\right) & \text{for } \alpha \geq 1/2, \end{cases} \tag{2}$$

see appendix A.1.3. The limiting cases are easily recovered by substitution, $\alpha = 0$ and $\alpha = 1$, in the first and second equation above, respectively.

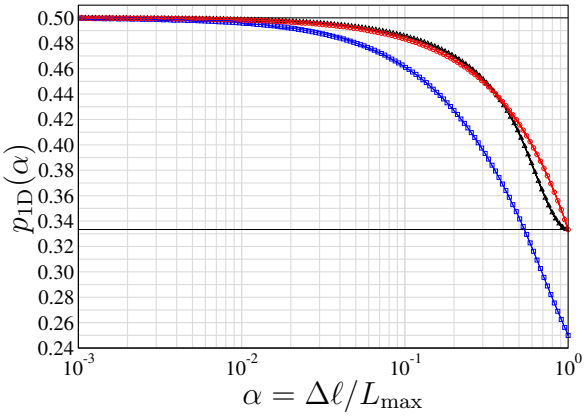

Figure 3: The probability of going forward $p_{1D}(\alpha)$ on an interval of length $L_{\max}$ versus the dimensionless ratio $\alpha = \Delta\ell/L_{\max}$ where $\Delta\ell$ is the maximum displacement between stopping positions and $L_{\max}$ is the maximum possible displacement. The lower horizontal line is $p_{1D}(\alpha) = \frac{1}{3}$, the value for $\alpha = 1$ while the upper horizontal line is $p_{1D}(\alpha) = \frac{1}{2}$, the limiting value for $\alpha \to 0$. The symbols display the results from a Monte Carlo simulation where the no. of stopping positions $M = 5 \cdot 10^5$ and the no. of samples $N = 1000$. The standard error of the mean $s \lesssim 2.5 \cdot 10^{-5}$ is less than the symbol size. The triangles, circles and squares represent the results from Monte Carlo simulations for the "no-go", "reflective" and "stop-go" boundary conditions. The solid lines superimposed over the symbols represent the associated analytic results in Eqs. (2), (18) and (25): the simulation results are in alignment with the analytical results.

5 Two-dimensional case

5.1 Definition of moving forward

Given three points $\mathbf{r}_1 = (x_1, y_1), \mathbf{r}_2 = (x_2, y_2)$ and $\mathbf{r}_3 = (x_3, y_3)$, we can define two vectors, namely the displacement vector $\mathbf{r}_{12} = \mathbf{r}_2 - \mathbf{r}_1$ from point $\mathbf{r}_1$ to point $\mathbf{r}_2$ and the displacement vector $\mathbf{r}_{23} = \mathbf{r}_3 - \mathbf{r}_2$ from point $\mathbf{r}_2$ to point $\mathbf{r}_3$ with coordinates

$$\mathbf{r}_{12} = \begin{pmatrix} x_2 - x_1 \\ y_2 - y_1 \end{pmatrix}; \quad \mathbf{r}_{23} = \begin{pmatrix} x_3 - x_2 \\ y_3 - y_2 \end{pmatrix}, \tag{3}$$

respectively, see Fig. 4. When the scalar product $\mathbf{r}_{12} \cdot \mathbf{r}_{23} > 0 \Leftrightarrow \cos\theta > 0$, where θ is the acute angle between the two vectors, the movement is forward. When the scalar product is negative or zero, that is, $\cos\theta \leq 0$, the movement is backwards, see Appendix B for further details. After the generic definition of moving forward, we will, in this section, focus on the "no-go" boundary condition but we also consider the "stop-go" and "reflective" boundary conditions for two dimensions in the appendix.

5.2 Circle and square with $\alpha = 1$

We can argue qualitatively why the probability to move forward in a confined space is affected by the boundary when the stopping points are chosen at random such that it is

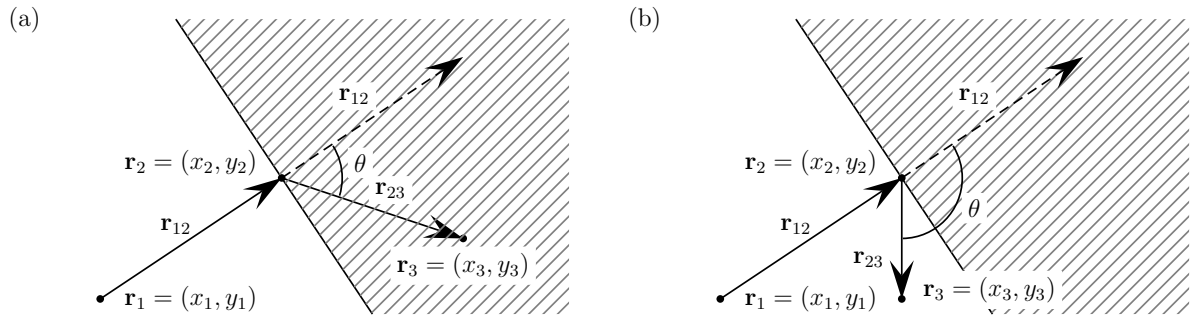

Figure 4: Three random points $\mathbf{r}_1, \mathbf{r}_2, \mathbf{r}_3$ with their two associated displacement vectors $\mathbf{r}_{12} = \mathbf{r}_2 - \mathbf{r}_1$ and $\mathbf{r}_{23} = \mathbf{r}_3 - \mathbf{r}_2$. The smallest angle θ, $0 \leq \theta \leq \pi$ between the two vectors $\mathbf{r}_{12}$ and $\mathbf{r}_{23}$ defines the direction of the vector $\mathbf{r}_{23}$ with respect to the vector $\mathbf{r}_{12}$. The hatched area with a boundary perpendicular to the vector $\mathbf{r}_{12}$ indicates the region where a stopping position $\mathbf{r}_3$ would imply forward movement. (a) Forward movement as $\mathbf{r}_{12} \cdot \mathbf{r}_{23} > 0 \Leftrightarrow \cos\theta > 0$. (b) Backward movement as $\mathbf{r}_{12} \cdot \mathbf{r}_{23} \leq 0 \Leftrightarrow \cos\theta \leq 0$.

not equal to 1/2.

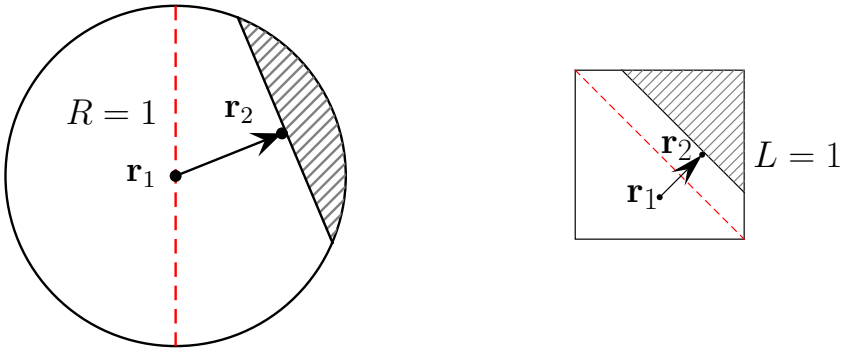

Figure 5: A unit circle with radius $R = 1$ and a unit square with sides $L = 1$. The dashed red lines indicate the diameter $L_{\max} = 2$ and the diagonal $L_{\max} = \sqrt{2}$, respectively. Three points $\mathbf{r}_1, \mathbf{r}_2$ and $\mathbf{r}_3$ are chosen at random and we define the two displacement vectors $\mathbf{r}_{12} = \mathbf{r}_2 - \mathbf{r}_1$ and $\mathbf{r}_{23} = \mathbf{r}_3 - \mathbf{r}_2$. The movement is forward if $\mathbf{r}_{12} \cdot \mathbf{r}_{23} > 0$ (see Fig. 4 and Appendix B), that is, if $\mathbf{r}_3$ is placed within the hatched area that has a boundary perpendicular to the vector $\mathbf{r}_{12}$.

Consider the situations when the confined region is either a circle or a square, see Fig. 5. After choosing two consecutive stopping points $\mathbf{r}_1$ and $\mathbf{r}_2$ at random, the hatched area within the confined region is where $\mathbf{r}_3$ has to be situated if the movement is forward. In the realisations displayed in Fig. 5, the fraction of the hatched areas is clearly less than $\frac{1}{2}$

of the total area. For other choices of $\mathbf{r}_1$ and $\mathbf{r}_2$, the probability of moving forward might be larger than 1/2 but this occurs less often.

We have derived an analytic expression for the probability of moving forward in a circle with diameter $L_{\max}$ when $\alpha = 1$, see Eq.(49b) in Appendix C.1. The analytical derivation is done for a circle with diameter $L_{\max}$, but the exact expression for the probability of going forward in a circle is independent of $L_{\max}$. By numerically integrating the analytical result, we find $p_{\bigcirc}(\alpha = 1) = 0.23990508\ldots$. For the case of a square with diagonal $L_{\max}$, we can apply the argument presented in Appendix C.2 to obtain the analytic result $p_{\square}(\alpha = 1) = 0.2417354\ldots$, which again is independent of the diagonal $L_{\max}$.

5.3 Circle and square with $0 < \alpha \leq 1$

When $\alpha = \Delta\ell/L_{\max} = 1$, the above results for $2D$ geometries assume that the stopping positions are chosen at random, that is, that the displacement between stopping positions has no restrictions except that stopping positions beyond the boundaries of the space are rejected, that is, we apply the "no-go" boundary condition.

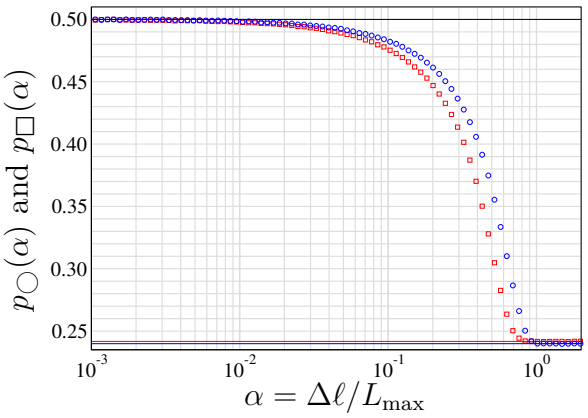

Figure 6: Numerical results for the probability of moving forward $p_{\bigcirc}(\alpha)$ and $p_{\square}(\alpha)$ in a circle with $L_{\max} = 2$ or square with $L_{\max} = \sqrt{2}$ with "no-go" boundary conditions, respectively, versus the dimensionless ratio $\alpha = \Delta\ell/L_{\max}$ where $\Delta\ell$ is the maximum displacement between stopping positions. Circle (blue circles): When $\alpha = 1$, the probability falls on the blue line with $p_{\bigcirc}(\alpha) = 0.23990508$. When decreasing α from 1 to 0, there is a crossover from $p_{\bigcirc}(\alpha) = 0.23990508$ to $p_{\bigcirc}(\alpha) = \frac{1}{2}$ indicated with the horizontal black line. Square (red squares): When $\alpha = 1$, the data falls on the red line with $p_{\square}(\alpha) = 0.2417354$. When decreasing α from 1 to 0, there is a crossover from $p_{\square}(\alpha) = 0.2417354$ to $p_{\square}(\alpha) = \frac{1}{2}$ indicated with the horizontal black line. In both cases, the number of samples for each data point $N = 100$, each with a sequence of $M = 10^5$ stopping points and the standard error of the mean $s \lesssim 2 \cdot 10^{-4}$ is less that the symbol sizes.

If we assume that the magnitude of the displacement between stopping positions is randomly chosen in the interval $[0, \alpha L_{\max}]$ for fixed $\alpha \in [0, 1]$, again under the restriction that they cannot be beyond the space boundary, then in numerical simulations for a unit circle with diameter $L_{\max} = 2$, we see a crossover from $p_{\bigcirc}(\alpha) = 0.23990508$ and $p_{\square}(\alpha) = 0.2417354$ for $\alpha = 1$ to $p_{\bigcirc}(\alpha) = p_{\square}(\alpha) = \frac{1}{2}$ for $\alpha \to 0$, see Fig. 6. We note that for most of the range $0 < \alpha \lesssim 0.9$, $p_{\square}(\alpha) < p_{\bigcirc}(\alpha)$ with a maximum difference of about 0.05 when $\alpha = 0.55$. The numerical data for the limiting value, $\alpha = 1$, provides χ^2 agreement with the analytical expressions for both circle and square.

5.4 Ellipse and rectangle with $0 < \alpha \leq 1$ and $0 \leq r \leq 1$

We can generalise the geometry from circle to ellipse and square to rectangle. We define the aspect ratio $0 \leq r \leq 1$ as the ratio between the minor and major axes of the ellipse and the smallest and largest sides in the rectangle, respectively. We denote the associated probabilities of moving forward by $p_{\bigcirc}(\alpha, r)$ and $p_{\square}(\alpha, r)$, respectively. For $r = 1$, we recover the circle and square. Hence, $p_{\bigcirc}(\alpha) = p_{\bigcirc}(\alpha, 1)$ and $p_{\square}(\alpha) = p_{\square}(\alpha, 1)$. We can also recover the one-dimensional case by setting $r = 0$, that is, $p_{\text{1D}}(\alpha) = p_{\bigcirc}(\alpha, 0) = p_{\square}(\alpha, 0)$.

We display the measured probability of going forward as a function α and the aspect ratio r of an ellipse and a rectangle in Fig. 7.

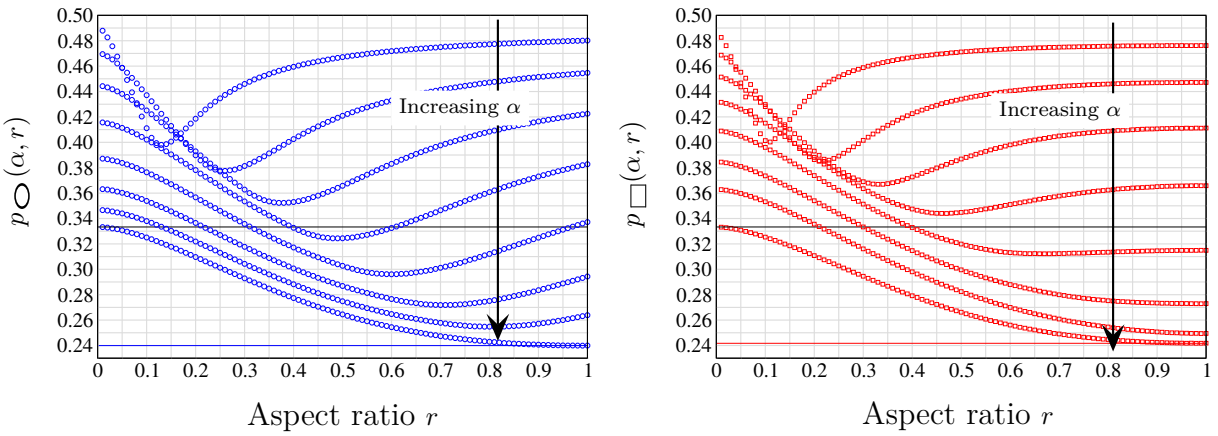

Figure 7: The probability of moving forward in an ellipse $p_{\bigcirc}(\alpha, r)$ (blue circles) and a rectangle $p_{\square}(\alpha, r)$ (red squares) with "no-go" boundary conditions versus the aspect ratio r for $\alpha = 1, 0.7, 0.6, 0.5, 0.4, 0.3, 0.2$, and 0.1, respectively. For $r = 1$, $p_{\bigcirc}(\alpha, 1) = 0.23990508$ (circle, indicated with the blue line) and $p_{\square}(\alpha, 1) = 0.2417354$ (square, indicated with the red line) while $p_{\bigcirc}(1, r) \to \frac{1}{3}$ and $p_{\square}(1, r) \to \frac{1}{3}$ (indicated with the upper black line) for $r \to 0$. The number of samples $N = 100$ with $M = 10^6$ randomly chosen points. The standard error of the mean $s \lesssim 5 \cdot 10^{-5}$ is smaller that the symbols.

For $r = 0$ (data on the y-axes), we recover the result obtained in Fig. 3, i.e., a crossover from $p_{\bigcirc}(1,0) = p_{\square}(1,0) = \frac{1}{3}$ to $p_{\bigcirc}(\alpha,0) = p_{\square}(\alpha,0) = \frac{1}{2}$ when $\alpha \to 0$. We notice that when α is not too large ($\alpha \lesssim 0.8$ for an ellispe and $\alpha \lesssim 0.5$ for a rectangle), there is a local minimum as a function of aspect ratio r.

One way of qualitatively understanding the presence of minima in the probability of moving forward as a function of the aspect ratio is to consider the 2D problem as a combination of two 1D problems, where movement is only allowed either along the first (x) or along the second (y) dimension. Starting from $r = 0$, as we increase the aspect ratio r, a new dimension becomes available for movement; however, this is initially much smaller than the maximum length of displacement between stops $\Delta\ell < L_{\max}$ and the overall probability is reduced (recall $p_{1\mathrm{D}}(\alpha)$ is a monotonically decreasing function of α). As the length available along the new dimension becomes comparable with $\Delta\ell$, the suppression of forward movement vanishes and the probability increases once again. In an approximation where the relative probability of moving in either direction is given by the aspect ratio, this qualitative model can be expressed as

$$p_{2\mathrm{D}}(\alpha, r) \simeq r\, p_{1\mathrm{D}}\left(\frac{\alpha L_{max}}{r}\right) + (1-r)\, p_{1\mathrm{D}}(\alpha L_{max}). \tag{4}$$

This approximation correctly reproduces the presence of minima and their approximate dependence on α, see Fig. 8. However, it fails to show that for sufficiently large $\Delta\ell/L_{max}$, the minima should disappear and the dependence on r becomes monotonic.

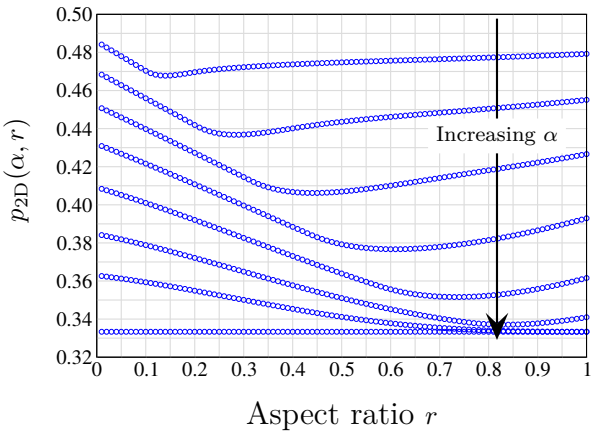

Figure 8: Aspect ratio dependence of the forward movement probability for "no-go" boundary conditions in 2D as expressed by Eq.(4) for $\alpha = \Delta\ell/L_{\max} = 1, 0.7, 0.6, 0.5, 0.4, 0.3, 0.2$ and 0.1. The approximation in Eq.(4) succeeds in reproducing the presence and approximate α dependence on the minima, although it fails to capture their numerical values or the absence of the minima for large α values.

5.5 Position probability in $2D$

For the simple random walk between stopping positions described in the sections above, we can find exact expressions for the probability density $g(x, y)\Delta x\Delta y$ for the random walker to be found within some infinitesimally small square with coordinates $x \in [x-\Delta x/2, x+\Delta x/2]$, $y \in [y-\Delta y/2, y+\Delta y/2]$ after some sufficiently long time from the beginning of the walk. This is done by calculating the overlap area of the circle of radius $\Delta\ell$ centred at (x, y) and the bounded space. In other words, the positions probability distribution (assumed to be time-independent for $M \gg 1$) is proportional to the "number of ways" the positions (x, y) can be accessed via a single displacement between stops. We can expect that a decrease in probability will be observed as we approach the boundary, due to a larger fraction of the space available for movement falling outside the allowed region, see Fig. 9 for an example of this effect. Although sometimes useful for analytical treatments, this result has an importance of its own in the context of empirical studies, as it warns us about the magnitude of purely geometrical effects on even the simplest observables.

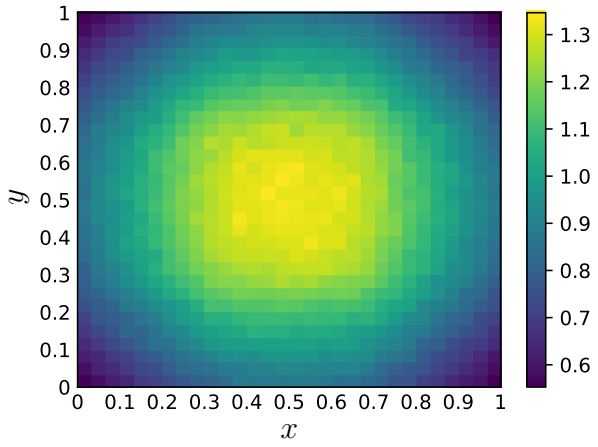

Figure 9: Colour-coded contour map showing a characteristic probability density $g(x, y)\Delta x\Delta y$ of stopping positions for a random walk on a unit square, $L_{\max} = \sqrt{2}$, with "no-go" boundary conditions, with a relative range of displacements between stops $\alpha = \Delta\ell/L_{\max} = 0.5$ and $\Delta x = \Delta y = 1/30$. The displayed data was produced in a single Monte Carlo run with $N = 10^7$. Note how the emerging positions distribution displays an approximate circular symmetry. The probability of a random walker to be in a given position increases with the number of points from which this position can be reached. Hence, this probability has a maximum in the centre and decays towards the boundary while its minima are in the four corners.

The same argument can be extended to bounded spaces of different dimensionality. In fact, knowledge of the exact form of the 1D probability $g(x)\Delta x$ was essential in solving the

1D case for general α, see Appendix A.1.3. A more thorough investigation of how position probabilities are affected by the geometrical properties of the boundary is presented in a companion paper [38].

6 Empirical applications

Experimentalists can estimate $\Delta\ell$ as the maximum displacement between the observed stopping positions and $L_{\max}$ as the maximum linear dimension of the bounded arena, territory or segregation area, such as the diameter for a circle or the diagonal for a square. Then they can use the value of $\alpha = \Delta\ell/L_{\max}$ to obtain the expected probability of moving forward, $p_{\mathcal{R}}(\alpha)$, from the tables we have provided. To test whether their study organism is more (or less) likely to move forward after a pause than expected from the null-model, they need to compare this expected probability with the 95% confidence interval for the proportion of forward movements between successive stop positions of their studied individual. If the expected probability value is outside the 95% confidence interval calculated from the data, there is at most a 5% chance that the organisation of the pauses in space is unstructured. Given such a small probability for the null hypothesis, it should be concluded that there is evidence for forward persistence or forward avoidance in the movement between stops.

In Appendix E, we describe a step-by-step procedure for testing whether there is forward persistence in the movement of an organism between successive stops. This procedure is based on the comparison between the observed and expected probability for moving forward. The observed probability is estimated empirically from the data and the expected probability is calculated from our null model which assumes no relationship between stopping points and hence no intrinsic forward persistence. We have produced six look-up tables for the expected probability, one for each of the two most common shapes of an experimental arena or a study area: the rectangle and the ellipse, under each of three boundary conditions (Tables S1-S6). In Tables S1-S2 ("no-go" boundary condition), the probability of moving forward can be looked up against (a) values of the aspect ratio $0 \leq r \leq 1$ of the rectangle or ellipse between 0.01 and 1.00 in steps of $\Delta r = 0.01$ and (b) values of the ratio $\alpha = \Delta\ell/L_{\max}$ between 0.01 and 1.00 in steps of $\Delta\alpha = 0.01$. In Tables S3-S6 ("stop-go" and "reflective" boundary conditions), probability values are available only for a square and a circle. Hence the aspect ratio, $r = 1$. Copies of Tables S1-S6 have been uploaded as supplementary material with the present paper.

The three boundary conditions are based on [35] and represent: stopping points chosen at random within the boundary ("no-go"), stopping at the boundary ("stop-go") and reflecting off the boundary ("reflective"). We describe the procedure and give two examples for each of the rectangular and elliptical shapes under the "no-go" boundary condition. One of the examples is for a value of $\Delta\ell/L_{\max}$ close to 1 ($\Delta\ell/L_{\max} = 0.81$, aspect ratio $r = 0.75$) and the other for a value of $\Delta\ell/L_{\max}$ close to 0 ($\Delta\ell/L_{\max} = 0.13$, $r = 0.15$).

The procedure is the same under the other two boundary conditions, except that the aspect ratio, $r = 1$ is constant. Please note that in Appendix D, Figure 17, we display the equivalent of Figure 6, but now for all three boundary conditions.

To calculate the empirical probability of moving forward, a rigorous definition of locomotion intermittence is necessary. We propose a definition originating in the study of ant movement tracked within the confines of the nest where the whole colony resides [13]. This approach is based on individual movement measured at short time intervals. Indeed, we can define the notion of a "stop-go" signal as a sequence of time intervals with movement ("go") interrupted by a sequence of time intervals with no movement, i.e., the recorded position remains exactly the same throughout a time interval ("stop") [13]. With the ever increasing technological possibilities for obtaining fine-grained tracking data in a variety of environments, this approach is applicable to the movement analysis of organisms across taxa.

Conclusions based on the step-by-step procedure are more reliable when the number of successive pairs of stops for an individual's trajectory is in the hundreds because the calculation of the 95% confidence interval for a proportion is based on a Gaussian approximation of the Binomial distribution.

When the geometry of the bounded space is not a circle, a square, an ellipse or a rectangle, empiricists could estimate the expected probability of moving forward between stops by using a bespoke methodology based on the principles of the Monte Carlo simulations described in Appendix D.

7 Discussion

A pause in locomotion might present an organism with the opportunity to make a decision about its next move. Here we presented a method for testing whether there is directional persistence between successive stops in individual intermittent locomotion in bounded space. Such directional persistence may mean that the organism uses stopping to make decisions about its next move or simply represent a body asymmetry that is conserved during inactivity. In either case establishing persistence is a necessary step before further investigation.

We analysed the spatio-temporal aspects of the sequence of stopping positions. The simplest possible observable here is whether or not the animal is moving forward from its current to its next stopping position. This is measured relatively to the direction defined by the movement from the previous to the present stopping position. When the maximum displacement between stopping points, $\Delta\ell$, is tiny relative to the linear dimension of the bounded space, $L_{\max}$, to all intents and purposes, the bounded region appears unbounded and the probability of moving forward is $\frac{1}{2}$. However, organisms are often kept in laboratory arenas whose linear dimension is easily within their movement

reach, which means that the ratio $\alpha = \Delta\ell/L_{\max}$ tends to 1. Therefore, the probability of moving forward within a bounded space is usually different from $\frac{1}{2}$. For example, for a circle and a square, we found $p_{\bigcirc}(\alpha) = 0.23990508$ and $p_{\square}(\alpha) = 0.24171354$, respectively when $\alpha = 1$ for the "no-go" boundary condition.

The beauty of our null model and the parameter $\alpha = \Delta\ell/L_{\max}$, in particular, is that it covers the whole spectrum of ratios between the max distance between the stopping positions ($\Delta\ell$) and the maximum dimension of the bounded space ($L_{\max}$). This includes the cases where the max distance between the stopping positions ($\Delta\ell$) is just a fraction of the maximum dimension of the bounded space ($L_{\max}$). For example, if we assume that the animal has an inherent max distance between the stopping positions, say $\Delta\ell_{\text{constant}}$, independent of the bounded space in which it is placed, then in experiments carried out in bounded spaces with increasing max dimension from $L_{\max} = \Delta\ell_{\text{constant}}$ and upwards, one would effectively be decreasing the parameter α from 1 downwards. Our model handles this case as it effectively amounts to the curve for $0 < \alpha \leq 1$ (Fig. 8). It is also important to remember that when α is close to 1, namely when the maximum distance between stopping positions is close to the maximum dimension of the bounded space, this maximum distance is the displacement between stops not the path. The path between stops is often convoluted and quite long. Hence, it is crucial that the positions between displacements represent stops in intermittent locomotion and not simply points of reorientation during continuous locomotion.

We also explored the effect of different boundary conditions on the probability of the animal moving forward betweeen stops. Our focus was on the "no-go" boundary condition [35]. According to this condition, the moving individual chooses an alternative position if the one already chosen is not within the bounded space. We focus on it because we do not expect many animals would have an increased probability of stopping at the boundary (the "stop-go" boundary condition) or would simply be reflected off the boundary (the "reflective" boundary condition). Even fewer would be able or willing to go through the boundary (the "absorbing" boundary condition) [35]. Nevertheless, the "stop-go" and "reflective" boundary conditions are possible particularly when an organism is exploring a novel space and interacting frequently with its boundary. In addition, it is well known that boundary conditions influence the behaviour of random walks differently [36, 35]. A more realistic, but also more complicated, is the "β-inelastic" boundary condition, which interpolates between the perfectly inelastic "stop-go" and the perfectly elastic "reflective" boundary conditions (for the analytic probability of moving forward in 1D under the "β-inelastic" boundary condition, please see A.3). Last, but not least, the boundary influences the distribution of the displacements between stops [38]. We cannot place an organism in a bounded space under the conditions described in this study and expect to measure the intrinsic distribution of displacements between stops.

The effect of environmental geometry on movement is still relatively unexplored. A recent study demonstrated the impact of shape on a trap's effectiveness in catching insects in relation to their movement characteristics [28]. Here we showed that geometry imposes a substantial external bias on the probability of moving forward within a bounded space such as an experimental arena. This finding provides an important null model for tests of directional persistence in the movement of organisms between stops during experiments. It is possible that our method could be extended, under certain conditions, to all points along the path of a moving organism. We focused specifically on the stopping points because they are selected by the studied organism itself and represent points along the path where some decision-making might be taking place. We hope the methodology developed in this paper will facilitate future empirical research into the movement of organisms as a window to understanding their decision-making processes.

Acknowledgements

K.C. would like to thank G. Pruessner for initial discussions on analytical calculations for the circle with $\alpha = 1$.

References

[1] Schwartz, A. B. (2016). Movement: how the brain communicates with the world. Cell, **164**(6), 1122-1135.

[2] Tinbergen, N. (1951). The study of instinct. Oxford: Oxford University Press.

[3] Okubo, A. (1980). Diffusion and Ecological Problems: Mathematical Models. (Biomathematics, Vol. **10**.) Berlin: Springer

[4] Turchin, P. (1998). Quantitative Analysis of Movement: Measuring and Modeling Population Redistribution in Animal and Plants. Sunderland, MA: Sinauer.

[5] Okubo, A. & Levin, S. A. (2001). Diffusion and Ecological Problems: Modern Perspectives. Mathematical Biology. Berlin: Springer.

[6] Benhamou, S. (2014). Of scales and stationarity in animal movements. Ecology letters, **17**(3), 261-272.

[7] Nathan, R., Getz, W. M., Revilla, E., Holyoak, M., Kadmon, R., Saltz, D., & Smouse, P. E. (2008). A movement ecology paradigm for unifying organismal movement research. Proceedings of the National Academy of Sciences, **105**(49), 19052-19059.

[8] O'Brien, W. J., Browman, H. I., & Evans, B. I. (1990). Search strategies of foraging animals. American Scientist, **78**(2), 152-160.

[9] Kramer, D. L., & McLaughlin, R. L. (2001). The behavioral ecology of intermittent

locomotion. American Zoologist, **41**(2), 137-153.

[10] Bartumeus, F., & Levin, S. A. (2008). Fractal reorientation clocks: Linking animal behavior to statistical patterns of search. Proceedings of the National Academy of Sciences, **105**(49), 19072-19077.

[11] Bartumeus, F. (2009). Behavioral intermittence, Lévy patterns, and randomness in animal movement. Oikos, **118**(4), 488-494.

[12] Peleg, O., & Mahadevan, L. (2016). Optimal switching between geocentric and egocentric strategies in navigation. Royal Society Open Science, 3(7), 160128.

[13] Christensen, K., Papavassiliou, D., de Figueiredo, A., Franks, N. R., & Sendova-Franks, A. B. (2015). Universality in ant behaviour. Journal of The Royal Society Interface, **12**(102), 20140985.

[14] Hunt, E. R., Baddeley, R. J., Worley, A., Sendova-Franks, A. B., & Franks, N. R. (2016). Ants determine their next move at rest: motor planning and causality in complex systems. Royal Society open science, **3**(1), 150534.

[15] Codling, E. A., Plank, M. J., & Benhamou, S. (2008). Random walk models in biology. Journal of the Royal Society Interface, **5**(25), 813-834.

[16] Maye, A., Hsieh, C. H., Sugihara, G., & Brembs, B. (2007). Order in spontaneous behavior. PloS one, **2**(5), e443.

[17] Anteneodo, C., & Chialvo, D. R. (2009). Unraveling the fluctuations of animal motor activity. Chaos: An Interdisciplinary Journal of Nonlinear Science, **19**(3), 033123.

[18] Benhamou, S., & Bovet, P. (1992). Distinguishing between elementary orientation mechanisms by means of path analysis. Animal Behaviour, **43**(3), 371-377.

[19] Wu, H. I., Li, B. L., Springer, T. A., & Neill, W. H. (2000). Modelling animal movement as a persistent random walk in two dimensions: expected magnitude of net displacement. Ecological Modelling, **132**(1-2), 115-124.

[20] Bailey, J. D., Wallis, J., & Codling, E. A. (2018). Navigational efficiency in a biased and correlated random walk model of individual animal movement. Ecology, **99**(1), 217-223.

[21] Kareiva, P. M., & Shigesada, N. (1983). Analyzing insect movement as a correlated random walk. Oecologia, **56**(2-3), 234-238.

[22] Marsh, L. M., & Jones, R. E. (1988). The form and consequences of random walk movement models. Journal of Theoretical Biology, **133**(1), 113-131.

[23] Benhamou, S. (2006). Detecting an orientation component in animal paths when the preferred direction is individual-dependent. Ecology, **87**(2), 518-528.

[24] Fagan, W. F., & Calabrese, J. M. (2014). The correlated random walk and the rise of movement ecology. The Bulletin of the Ecological Society of America, **95**(3), 204-206.

[25] Patlak, C. S. (1953). Random walk with persistence and external bias. The bulletin of mathematical biophysics, **15**(3), 311-338.

[26] Sendova-Franks, A. B., & Van Lent, J. (2002). Random walk models of worker sorting in ant colonies. Journal of Theoretical Biology, **217**(2), 255-274.

[27] Jeanson, R., Blanco, S., Fournier, R., Deneubourg, J. L., Fourcassié, V., & Theraulaz, G. (2003). A model of animal movements in a bounded space. Journal of Theoretical Biology, **225**(4), 443-451.

[28] Ahmed, D. A., & Petrovskii, S. V. (2019). Analysing the impact of trap shape and movement behaviour of ground-dwelling arthropods on trap efficiency. Methods in Ecology and Evolution, **10**(8), 1246-1264.

[29] Giuggioli, L., Potts, J. R., & Harris, S. (2011). Animal interactions and the emergence of territoriality. PLoS Comput Biol, **7**(3), e1002008.

[30] Potts, J. R., & Lewis, M. A. (2014). How do animal territories form and change? Lessons from 20 years of mechanistic modelling. Proceedings of the Royal Society of London B: Biological Sciences, **281**(1784), 20140231.

[31] Riotte-Lambert, L., Benhamou, S., & Chamaillé-Jammes, S. (2015). How memory-based movement leads to nonterritorial spatial segregation. The American Naturalist, **185**(4), E103-E116.

[32] Russell, J. C., McMorland, A. J., & MacKay, J. W. (2010). Exploratory behaviour of colonizing rats in novel environments. Animal Behaviour, **79**(1), 159-164.

[33] von Merten, S., & Siemers, B. M. (2012). Exploratory behaviour in shrews: fast-lived *S*orex versus slow-lived *C*rocidura. Animal Behaviour, **84**(1), 29-38.

[34] Degen, J., Kirbach, A., Reiter, L., Lehmann, K., Norton, P., Storms, M., Koblofsky, M., Winter, S., Georgieva, P.B., Nguyen, H. & Chamkhi, H. (2015). Exploratory behaviour of honeybees during orientation flights. Animal Behaviour, **102**, 45-57.

[35] Bearup, D., & Petrovskii, S. (2015). On time scale invariance of random walks in confined space. Journal of theoretical biology, **367**, 230-245.

[36] Hernandez-Garcia, E., Pesquera, L., Rodriguez, M. A., & San Miguel, M. (1987). First-passage time statistics: processes driven by Poisson noise. Physical Review A, **36**, 5774-5781.

[37] Adhikari, S. K. (1981). Iterative solution of homogeneous integral equations. Journal of Computational Physics, **43**, 189-193.

[38] Cocconi, L., Kuhn-Régnier, A., Neuss, M., Christensen, K. & Sendova-Franks, A. B. (2020). Reconstruction of the intrinsic statistical properties of a random walk through compensation for boundary effects. Under review.

A Analytic calculation in $1D$

A.1 "No-go" boundary condition

A.1.1 Interval with $\alpha = 1$

The probability density for choosing a point at random in an interval is uniform, that is, if the interval is $[0, L]$, then

$$P(x)dx = \frac{1}{L}dx, \tag{5a}$$

such that

$$\int_0^L P(x)dx = 1. \tag{5b}$$

In 1D, $L_{\max} = L$ so $\alpha = \Delta\ell/L_{\max} = 1$ is associated with $\Delta\ell = L$. We can calculate the associated probability that $x_1 \in [0, L]$, $x_2 \in]x_1, L]$ and $x_3 \in]x_2, L]$:

$$\begin{aligned}
P(x_3 > x_2 > x_1) &= \int_0^L \frac{1}{L}dx_1 \int_{x_1}^L \frac{1}{L}dx_2 \int_{x_2}^L \frac{1}{L}dx_3 \\
&= \frac{1}{L^3}\int_0^L dx_1 \int_{x_1}^L dx_2 \,[x_3]_{x_2}^L \\
&= \frac{1}{L^3}\int_0^L dx_1 \int_{x_1}^L (L - x_2)dx_2 \\
&= \frac{1}{L^3}\int_0^L dx_1 \left[Lx_2 - \frac{1}{2}x_2^2\right]_{x_1}^L \\
&= \frac{1}{L^3}\int_0^L \left(\frac{1}{2}L^2 - Lx_1 + \frac{1}{2}x_1^2\right) dx_1 \\
&= \frac{1}{L^3}\left[\frac{1}{2}L^2x_1 - \frac{1}{2}Lx_1^2 + \frac{1}{6}x_1^3\right]_0^L \\
&= \frac{1}{6},
\end{aligned} \tag{6a}$$

and similarly for $x_1 \in [0, L]$, $x_2 \in\ [0, x_1[$ and $x_3 \in\ [0, x_2[$:

$$P(x_3 < x_2 < x_1) = \int_0^L \frac{1}{L}dx_1 \int_0^{x_1} \frac{1}{L}dx_2 \int_0^{x_2} \frac{1}{L}dx_3 = \frac{1}{6}. \tag{6b}$$

Hence, the probability of going forward in 1D is

$$p_{1\mathrm{D}}(\alpha) = P(x_3 > x_2 > x_1) + P(x_3 < x_2 < x_1) = \frac{1}{3}, \tag{7}$$

when $\alpha = 1$. This result holds for *any* finite interval of length L in 1D.

A.1.2 Interval with $\alpha \to 0$

We will show that in the limit of $\alpha \to 0$, the probability of going forward equals $\frac{1}{2}$. When $\alpha \ll 1$, the stopping position x_2 is within an interval of length $2\Delta\ell$ centered around x_1. Likewise, the stopping position x_3 is within an interval of length $2\Delta\ell$ centered around x_2. The associated probability density for choosing a point at random within such an interval is uniform, that is,

$$P(x)dx = \frac{1}{2\Delta\ell}dx, \tag{8a}$$

such that

$$\int_{x_1-\Delta\ell}^{x_1+\Delta\ell} P(x)dx = 1, \tag{8b}$$

and similarly for an interval of length $2\Delta\ell$ around x_2. We can calculate the associated probability that $x_1 \in [0, L]$, $x_2 \in]x_1, x_1 + \Delta\ell]$ and $x_3 \in]x_2, x_2 + \Delta\ell]$:

$$\begin{aligned} P(x_3 > x_2 > x_1) &= \int_0^L \frac{1}{L}dx_1 \int_{x_1}^{x_1+\Delta\ell} \frac{1}{2\Delta\ell}dx_2 \int_{x_2}^{x_2+\Delta\ell} \frac{1}{2\Delta\ell}dx_3 \\ &= \frac{1}{L\,(2\Delta\ell)^2} \int_0^L dx_1 \int_{x_1}^{x_1+\Delta\ell} dx_2\,[x_3]_{x_2}^{x_2+\Delta\ell} \\ &= \frac{1}{4L\Delta\ell} \int_0^L dx_1 \int_{x_1}^{x_1+\Delta\ell} dx_2 \\ &= \frac{1}{4L} \int_0^L dx_1 \\ &= \frac{1}{4}, \end{aligned} \tag{9a}$$

and similarly for $x_1 \in [0, L]$, $x_2 \in\ [x_1 - \Delta\ell, x_1[$ and $x_3 \in\ [x_2 - \Delta\ell, x_2[$:

$$P(x_3 < x_2 < x_1) = \frac{1}{4}. \tag{9b}$$

Hence, the probability of going forward in 1D is

$$p_{1\mathrm{D}}(\alpha) = P(x_3 > x_2 > x_1) + P(x_3 < x_2 < x_1) = \frac{1}{2}, \tag{10}$$

when $\alpha \to 0$. This result holds for *any* interval of length L in 1D.

A.1.3 Interval with $0 < \alpha \leq 1$

We consider the sequence of stopping positions in terms of triplets of time-ordered coordinates x_{i-1}, x_i, x_{i+1}. We then calculate the probability density $g(x; \alpha)$ for the central point of a particular triplet to be located at coordinate x along the 1D segment for a given $\alpha = \Delta\ell/L_{\max}$. One can find these distributions by considering the number of "ways-in"

for each point along the segment, that is, the number of points in the segment that can be reached in a single displacement between stops. For $\alpha \leq 1/2$ we obtain

$$g\left(x;\alpha \leq 1/2\right) \propto \begin{cases} \dfrac{x+\alpha}{2\alpha} & \text{for } x \in [0,\alpha], \\ 1 & \text{for } x \in [\alpha, 1-\alpha], \\ \dfrac{(1-x)+\alpha}{2\alpha} & \text{for } x \in [1-\alpha, 1], \end{cases} \tag{11}$$

while for $\alpha > 1/2$ we obtain

$$g\left(x;\alpha > 1/2\right) \propto \begin{cases} \dfrac{x+\alpha}{2\alpha} & \text{for } x \in [0,1-\alpha], \\ \dfrac{1}{2\alpha} & \text{for } x \in [1-\alpha, \alpha], \\ \dfrac{(1-x)+\alpha}{2\alpha} & \text{for } x \in [\alpha, 1]. \end{cases} \tag{12}$$

The next step is to calculate the probability $p(x;\alpha)$ for the previous and next stopping positions to be found on opposite sides of a central point located at x, which is an equivalent description of forward movement in 1D. This is done by considering the lengths available for movement on either side of the central point, let's call these ℓ_x and r_x, with the probability being given by $2(\ell_x r_x)/(\ell_x + r_x)^2$. This approach gives for $\alpha \leq 1/2$

$$p(x;\alpha \leq 1/2) = \begin{cases} \dfrac{2x\alpha}{(x+\alpha)^2} & \text{for } x \in [0,\alpha], \\ \dfrac{1}{2} & \text{for } x \in [\alpha, 1-\alpha], \\ \dfrac{2(1-x)\alpha}{(x+\alpha)^2} & \text{for } x \in [1-\alpha, 1], \end{cases} \tag{13}$$

and for $\alpha > 1/2$

$$p(x;\alpha > 1/2) = \begin{cases} \dfrac{2x\alpha}{(x+\alpha)^2} & \text{for } x \in [0,1-\alpha], \\ 2x(1-x) & \text{for } x \in [1-\alpha, \alpha], \\ \dfrac{2(1-x)\alpha}{(x+\alpha)^2} & \text{for } x \in [\alpha, 1]. \end{cases} \tag{14}$$

We can now calculate the probability of forward movement $p_{1\mathrm{D}}(\alpha)$ for a random walk on a 1D segment as a function of α by weighting Eq. (13) and Eq.(14) by Eq.(11) and Eq.(12), respectively. This is done via the integral

$$p_{1\mathrm{D}}(\alpha) = \int_0^1 g(x;\alpha)p(x;\alpha)\, dx, \tag{15}$$

which can be evaluated to give the exact expression valid on the full range $0 < \alpha \leq 1$

$$p_{\mathrm{1D}}(\alpha) = \begin{cases} \dfrac{1 + 2\alpha(1 - 2\log(2))}{2 - \alpha} & \text{for } \alpha \leq 1/2, \\ \dfrac{4}{2 - \alpha}\left(1 + \alpha \log \alpha - \dfrac{6\alpha^2 + 4\alpha^3 + 1}{12\alpha}\right) & \text{for } \alpha \geq 1/2. \end{cases} \tag{16}$$

The limiting cases mentioned previously are easily recovered by substitution, $\alpha = 0$ and $\alpha = 1$, in the first and second equation above, respectively.

A.2 "Reflective" boundary condition

In the case of "reflective" boundary conditions in $d = 1$, the steady-state stopping position probability distribution is uniform. On the unit segment, we thus have $g(x; \alpha) = 1$. One can convince themselves of this result by noting that "reflective" and periodic boundaries are dynamically equivalent and, consequently, the steady-state should be invariant under spatial translation within the segment. Following the same procedure as above, we now calculate the conditional forward movement probability $p(x_i; \alpha)$ for a given mid-point x_i of the ordered triplet x_{i-1}, x_i, x_{i+1}. For simplicity we only consider the case $\alpha \leq 1$. This conditional probability is given by

$$p(x_i; \alpha) = \begin{cases} 1/2 & \text{if } \alpha/2 < x_i \leq 1/2, \\ \frac{2x(\alpha - x)}{\alpha^2} & \text{if } x_i \leq \alpha/2, \end{cases} \tag{17}$$

with $p(x_i; \alpha) = p(1 - x_i; \alpha)$ by symmetry. The space-averaged probability of forward movement is therefore given by

$$P_F(\alpha) = \frac{1}{2}(1 - \alpha) + 2\int_0^{\alpha/2} dx \ \left(\frac{2x}{\alpha} - \frac{2x^2}{\alpha^2}\right) = \frac{1}{2}(1 - \alpha/3). \tag{18}$$

For $\alpha \to 0$, this converges to the value $1/2$, characteristic of movement in an unbounded space. For $\alpha = 1$ "reflective" and "no-go" boundary conditions produce identical dynamics and we correctly get the probability $P_F(1) = 1/3$ derived earlier for the latter case.

A.3 "Stop-go" boundary condition

In the case of "stop-go" boundary conditions, the challenge (already in $d = 1$) is to obtain the steady-state stopping position distribution. Unlike for "reflective" and "no-go" boundaries, here we need to define and treat the probabilities $g(0; \alpha)$ and $g(1; \alpha)$ for the random walker to be found at the boundaries separately. Restricting ourselves to the case $0 < \alpha \leq 1$, the discrete-time evolution of the stopping position distribution from an arbitrary initial condition $\{g^{(0)}(x; \alpha), g^{(0)}(0; \alpha), g^{(0)}(1; \alpha)\}$ with $x \in (0, 1)$ is given by the

system of recurrence relations

$$g^{(n+1)}(x;\alpha) = \frac{\theta(\alpha - x)}{2\alpha} g^{(n)}(0;\alpha) + \frac{\theta(x - 1 + \alpha)}{2\alpha} g^{(n)}(1;\alpha) + \int_0^1 dx' \; \frac{\theta(x' - x + \alpha)\theta(x + \alpha - x')}{2\alpha} g^{(n)}(x';\alpha), \tag{19a}$$

$$g^{(n+1)}(0;\alpha) = \frac{1}{2} g^{(n)}(0;\alpha) + \int_0^1 dx' \; \frac{\alpha - x'}{2\alpha} \theta(\alpha - x') g^{(n)}(x';\alpha), \tag{19b}$$

$$g^{(n+1)}(1;\alpha) = \frac{1}{2} g^{(n)}(1;\alpha) + \int_0^1 dx' \; \frac{x' - 1 + \alpha}{2\alpha} \theta(x' - 1 + \alpha) g^{(n)}(x';\alpha). \tag{19c}$$

At stationarity, $g^{(n)} = g^{(n+1)} = g^{(\infty)}$ and the above system of equations reduces to a single integral equation, specifically a homogeneous Fredholm equation of the second kind, for the steady-state stopping position distribution of the form

$$g^{(\infty)}(x;\alpha) = \int_0^1 dx' \; K(x, x';\alpha) g^{(\infty)}(x';\alpha), \tag{20}$$

with integration kernel

$$K(x, x';\alpha) = \frac{1}{2\alpha} \big[\theta(x' - x + \alpha)\theta(x + \alpha - x') + \frac{\alpha - x'}{\alpha} \theta(\alpha - x')\theta(\alpha - x) + \frac{x' - 1 - \alpha}{\alpha} \theta(x' - 1 + \alpha)\theta(x - 1 + \alpha) \big]. \tag{21}$$

Equation (20) is invariant under multiplication of $g^{(\infty)}$ by a constant and a normalisation condition thus needs to be provided of the form

$$\int_0^1 dx \left(1 + \frac{2(x - 1 + \alpha)}{\alpha} \theta(x - 1 + \alpha) \right) g^{(\infty)}(x;\alpha) = 1. \tag{22}$$

We note in passing that (22) can be used to recast (20) as an inhomogeneous Fredholm integral equation of the second kind [37] of the form

$$g^{(\infty)}(x;\alpha) = K(x, x_0;\alpha) + \int_0^1 dx' \; K'(x, x';\alpha) g^{(\infty)}(x';\alpha), \tag{23}$$

with $x_0 \in (0, 1)$ an arbitrary bulk point and the modified integration kernel

$$K'(x, x';\alpha) = K(x, x';\alpha) - K(x, x_0;\alpha) \left(1 + \frac{2(x' - 1 + \alpha)}{\alpha} \theta(x' - 1 + \alpha) \right). \tag{24}$$

This transformation is convenient for the purpose of determining the steady-state numerically. However, since we don't expect that the steady-state stopping distribution

can be obtained in closed form, we take the simpler route of evolving an initial uniform distribution to a numerical steady-state by iterating (21). With this information at hand, it is sufficient to note that the conditional forward movement probability $p(x_i;\alpha)$ given the mid-point x_i of an ordered triplet x_{i-1}, x_i, x_{i+1} is equal to $1/2$ for all bulk points $x_i \in (0,1)$ and vanishes for $x_i \in \{0,1\}$ (with the convention that $x_{i+1} = x_i$ counts as a backwards displacement between stops). Thus, the position-averaged forward movement probability is given by

$$P_F(\alpha) = \frac{1}{2}\int_0^1 dx\ g^{(\infty)}(x;\alpha). \tag{25}$$

For the limiting case $\alpha = 1$, exactly half the mass of the jump kernel extends outside of the domain independently of the starting position of the jump. The probability for the random walker to be found anywhere in the bulk after a jump is therefore $1/2$, thus $P_F(1) = 1/4$.

A.4 β-inelastic boundary condition

As it turns out, "stop-go" and "reflective" boundary conditions can be understood as special cases of a more general class of boundary conditions [35], which we here refer to as β-inelastic. This one-parameter family of boundary conditions interpolates between perfectly inelastic ("stop-go") and perfectly elastic ("reflective") by introducing a "damping factor" $\beta \in (0,1]$, multiplying the remaining length of the jump after reflection at the boundary. For $\beta = 1$ one recovers elastic reflection, for $\beta \to 0$ jumps are terminated infinitesimally close to the boundary. Taking the limit $\beta \to 0$ rather than setting $\beta = 0$ is required to avoid ambiguities arising when $x_i = x_{i+1}$. Restricting ourselves to the case $0 < \alpha \leq 1$, the discrete-time evolution of the stopping position distribution from an arbitrary initial condition $g^{(0)}(x;\alpha,\beta)$ with $x \in (0,1)$ is given by the recurrence relations $g^{(n+1)}(x;\alpha;\beta) = \int_0^1 dx'\ K(x,x';\alpha,\beta)g^{(n)}(x';\alpha,\beta)$ with integration kernel

$$K(x,x';\alpha,\beta) = \frac{\theta(x-x'+\alpha)\theta(x'+\alpha-x)}{2\alpha} + \frac{\theta(\beta(\alpha-x')-x)}{2\alpha/\beta} + \frac{\theta(x-1+\beta(x'+\alpha-1))}{2\alpha/\beta}. \tag{26}$$

At stationarity, $g^{(n)} = g^{(n+1)} = g^{(\infty)}$ and the corresponding homogeneous Fredholm equation for the steady-state stopping position distribution reads $g^{(\infty)}(x;\alpha,\beta) = \int_0^1 dx'\ K(x,x';\alpha,\beta)g^{(\infty)}(x';\alpha,\beta)$ with the normalisation condition $\int_0^1 dx\ g^{(\infty)}(x;\alpha,\beta) = 1$. Again, we can use this normalisation to recast the steady-state equation in an inhomogeneous form as

$$g^{(\infty)}(x;\alpha,\beta) = K(x,x_0;\alpha,\beta) + \int_0^1 dx'(K'(x,x';\alpha,\beta) - K(x,x_0;\alpha,\beta))g^{(\infty)}(x';\alpha,\beta) \tag{27}$$

with $x_0 \in (0,1)$ an arbitrary bulk point. Having solved for the steady-state stopping position distribution, one then needs to evaluate the conditional forward movement probability $p(x_i;\alpha,\beta)$ for a given the mid-point x_i of the ordered triple x_{i-1}, x_i, x_{i+1}. Due to the

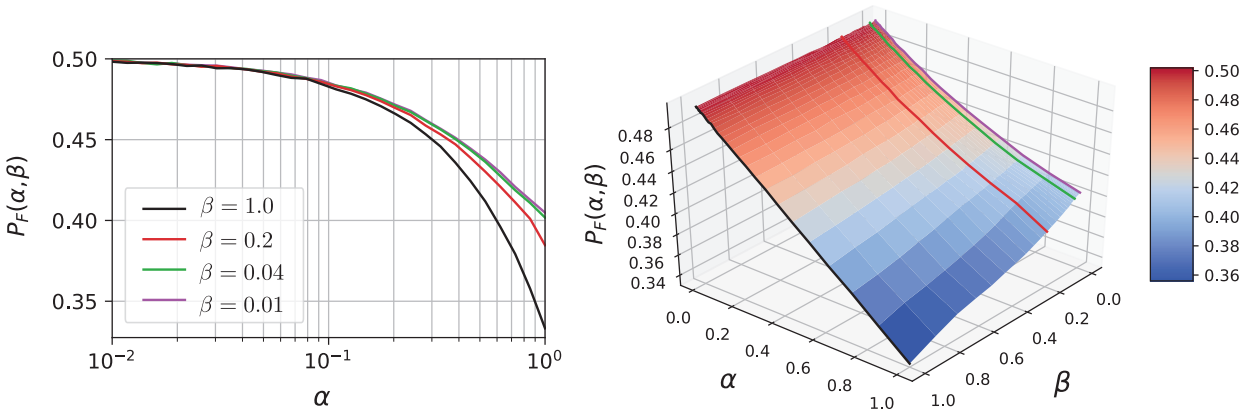

Figure 10: For β-inelastic boundary conditions, the probability of going forward $P_F(\alpha, \beta)$ on an interval of length $L_{\max}$ depends both on the dimensionless ratio $\alpha = \Delta\ell/L_{\max}$, with $\alpha \in [0, 1]$, and on the damping factor β, with $\beta \in (0, 1]$. Left: forward movement probability as a function of α for a set of representative values of β ($\beta = 1$ is equivalent to reflecting boundary conditions). Right: full dependence of the forward movement probability on both parameters α and β. For comparison, the curves plotted in the left panel are traced with matching colors.

dissipative nature of the inelastic interactions with the boundary, time reversal symmetry is broken in the dynamics (unlike "reflective" and "no-go" boundaries) and $p(x_i; \alpha, \beta)$ depends explicitly on the steady-state stopping distribution. Introducing the time-reversed jump kernel $K^R(x, x'; \alpha, \beta) \propto K(x', x; \alpha, \beta) g^{(\infty)}(x; \alpha, \beta)$ with $\int dx\ K^R(x, x'; \alpha, \beta) = 1$, we can write the conditional forward movement probability as

$$p(x_i; \alpha, \beta) = \int_0^{x_i} dy\ K(y, x_i; \alpha, \beta) \int_{x_i}^1 dy'\ K^R(y', x_i; \alpha, \beta) + \int_0^{x_i} dy\ K^R(y, x_i; \alpha, \beta) \int_{x_i}^1 dy'\ K(y', x_i; \alpha, \beta). \tag{28}$$

The position-average forward movement probability is thus given by $P_F(\alpha, \beta) = \int_0^1 dx\ p(x; \alpha, \beta) g^{(\infty)}(x; \alpha, \beta)$.

B Finding θ with a sign in $2D$

The dot product (scalar product) of the two vectors (see Fig.4)

$$\mathbf{r}_{12} \cdot \mathbf{r}_{23} = \begin{pmatrix} x_2 - x_1 \\ y_2 - y_1 \end{pmatrix} \cdot \begin{pmatrix} x_3 - x_2 \\ y_3 - y_2 \end{pmatrix} = (x_2 - x_1)(x_3 - x_2) + (y_2 - y_1)(y_3 - y_2), \tag{29}$$

allows us to determine the (absolute) value of the angle θ via the equation

$$\cos\theta = \frac{\mathbf{r}_{12}\cdot\mathbf{r}_{23}}{|\mathbf{r}_{12}|\,|\mathbf{r}_{23}|} \quad \text{with } 0 \leq \theta \leq \pi, \tag{30}$$

where the lengths of the two vectors appear in the denominator

$$|\mathbf{r}_{12}| = \sqrt{(x_2 - x_1)^2 + (y_2 - y_1)^2}, \tag{31a}$$

$$|\mathbf{r}_{23}| = \sqrt{(x_3 - x_2)^2 + (y_3 - y_2)^2}. \tag{31b}$$

From Eq.(30) we can then determine the angle θ where $0 \leq \theta \leq \pi$, allowing us to characterize the movement as forward or backward

$$\text{Forward} \Leftrightarrow \mathbf{r}_{12}\cdot\mathbf{r}_{23} > 0 \Leftrightarrow \theta < \pi/2, \tag{32a}$$

$$\text{Backward} \Leftrightarrow \mathbf{r}_{12}\cdot\mathbf{r}_{23} \leq 0 \Leftrightarrow \theta \geq \pi/2. \tag{32b}$$

We can define θ with a sign such that if the vector $\mathbf{r}_{23}$ is to the right of $\mathbf{r}_{12}$ (as in the examples in Fig.4), $-\pi < \theta < 0$. Similarly, if the vector $\mathbf{r}_{23}$ is to the left of $\mathbf{r}_{12}$, $0 < \theta < \pi$. If the vectors are pointing in the same (opposite) direction, $\theta = 0(\pm\pi)$. Hence, forward direction has $-\pi/2 < \theta < \pi/2$ and backwards direction has $-\pi \leq \theta \leq -\pi/2$ or $\pi/2 \leq \theta \leq \pi$. The angle θ determined from Eq.(30) does not contain information about the sign of the angle, that is, if we have a forward direction $\theta < \pi/2$, we do not know if the vector $\mathbf{r}_{23}$ is pointing to the left or to the right of the vector $\mathbf{r}_{12}$. However, the sign of θ is identical to the sign of a quantity derived from the cross-product of associated vectors in $\mathbb{R}^3$, that is, the vectors $\mathbf{r}_{12}$ and $\mathbf{r}_{23}$ with an added zero third coordinate. Let us call this quantity C where

$$C = (x_2 - x_1)(y_3 - y_2) - (x_3 - x_2)(y_2 - y_1). \tag{33}$$

The angle θ should take the sign of C, that is, if $C > 0$ then $\theta > 0$, if $C < 0$ then $\theta < 0$. If $C = 0$ then $\theta = 0$ or $\theta = \pm\pi$. Hence, the algorithm to determine the angle θ with a sign in $2D$ is:

1. Determine the two vectors $\mathbf{r}_{12}$ and $\mathbf{r}_{23}$ from the three points, see Eq.(3).

2. Calculate their dot-product from Eq.(29) and their lengths Eqs.(31) and use Eq.(30) to determine the angle θ, $0 \leq \theta \leq \pi$.

3. Calculate the quantity C from Eq.(33). If $C < 0$, θ is negative, i.e., set $\theta = -\theta$. If $C \geq 0$ do nothing.

Then θ will be measured with a sign according to the definition given in Fig.4.

C Analytic calculation in $2D$

C.1 Exact result for circle with $\alpha = 1$

We will now derive an analytic result for the case of a circle with radius R_0, i.e., $L_{\max} = 2R_0$. The symmetry of the circle makes it simpler to consider than the square.

Assume the centre of the circle is at the origin of a 2D coordinate system. We now choose two points $\mathbf{r}_1$ and $\mathbf{r}_2$ at random. Due to symmetry, we can, without loss of generality, assume that the point $\mathbf{r}_1$ is on the positive x-axis. Similarly, we may assume that the point $\mathbf{r}_2$ has $y \geq 0$. A point $\mathbf{r}_2$ with a negative y-coordinate behaves identically as can be seen from a reflection in the y-axis. We will follow a calculation suggested by G. Pruessner (private communication).

Let us define the radius and angles associated with the random points via

$$\mathbf{r}_i = r_i(\cos(\phi_i), \sin(\phi_i))), \quad \text{for } i = 1, 2, \ldots \tag{34}$$

where by definition $\phi_1 = 0$. Because $y \geq 0$, the angle $0 \leq \phi_2 \leq \pi$.

We now need to consider the two different cases:

1. Fig.11: $0 \leq \phi_2 \leq \pi/2$; $r_2 > r_1 \cos\phi_2$ or $r_2 < r_1 \cos\phi_2$,
2. Fig.12: $\pi/2 \leq \phi_2 \leq \pi$.

First, we will find the area $A(R, R_0)$ of the hatched segment, where we define R as the distance of the chord with length $2c$ from the origin of the circle with radius R_0. From the geometry of the two identical triangles with sides R, c and R_0 we have

$$R^2 + c^2 = R_0^2 \Leftrightarrow 2c = 2\sqrt{R_0^2 - R^2}. \tag{35}$$

This equation is generic, that is, it is true in Fig.11 and Fig.12. In Fig.11(a) and in Fig.12, the area of the hatched region is

$$\begin{aligned} A(R, R_0) &= \int_R^{R_0} 2\sqrt{R_0^2 - r^2}\, dr \\ &= R_0^2 \int_{R/R_0}^1 2\sqrt{1-u^2}\, du \quad \text{with } u = r/R_0 \\ &= R_0^2 \left[u\sqrt{1-u^2} + \sin^{-1} u\right]_{R/R_0}^1 \\ &= R_0^2 \left(\cos^{-1}(R/R_0) - \frac{R}{R_0}\sqrt{1-(R/R_0)^2}\right), \end{aligned} \tag{36}$$

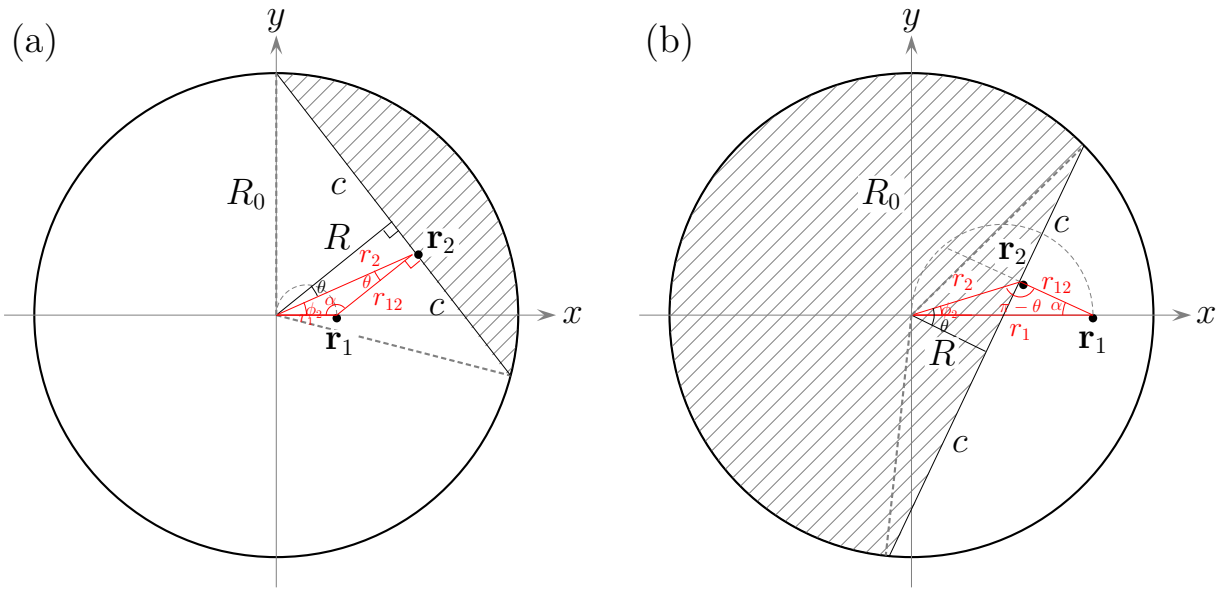

Figure 11: A circle with radius R_0 centered in the origin of a coordinate system oriented such that the point $\mathbf{r}_1$ is on the positive x-axis and the randomly chosen point $\mathbf{r}_2$ has $y \geq 0, 0 \leq \phi_2 \leq \pi/2$. The boundary of the hatched segment is defined by the chord that is perpendicular to the vector $\mathbf{r}_{12} = \mathbf{r}_2 - \mathbf{r}_1$ and passes through the point $\mathbf{r}_2$. If $\mathbf{r}_3$ falls within the hatched segment, then $\mathbf{r}_{12} \cdot \mathbf{r}_{23} > 0$ and the movement is forward. (a) $r_2 > r_1 \cos\phi_2$, i.e., in the first quadrant but outside the half-circle outlined with dashed gray line. Geometry reveals that $r_2 = r_{12}\cos\theta + r_1 \cos\phi_2$. (b) $r_2 < r_1 \cos\phi_2$, i.e., in the first quadrant but inside the half-circle outlined with dashed gray line. Geometry reveals that $r_2 = r_1 \cos\phi_2 - r_{12}\cos\theta$.

where we in the last step identify $\cos^{-1}(R/R_0) = \frac{\pi}{2} - \sin^{-1}(R/R_0)$. In the limits we find $A(0, R_0) = \pi R_0^2/2$ and $A(R_0, R_0) = 0$ as expected. However, in Fig.11(b), the area of the hatched region is

$$A^+(R, R_0) = \pi R_0^2 - A(R, R_0). \tag{37}$$

In the limits we find $A^+(0, R_0) = \pi R_0^2/2$ and $A^+(R_0, R_0) = \pi R_0^2$ as expected. Note that $A^+(R, R_0) = A(-R, R_0)$ because $\cos^{-1}(x) + \cos^{-1}(-x) = \pi$.

Now, we want to express $R(r_1, r_2, \phi_2)$, where from the geometry

$$R\,(r_1, r_2, \phi_2) = r_2 \cos\theta. \tag{38}$$

In the three different cases, we have

$$r_2 = \begin{cases} r_1 \cos\phi_2 + r_{12}\cos\theta, \\ r_1 \cos\phi_2 - r_{12}\cos\theta, \\ r_1 \cos\phi_2 + r_{12}\cos\theta, \end{cases} \tag{39}$$

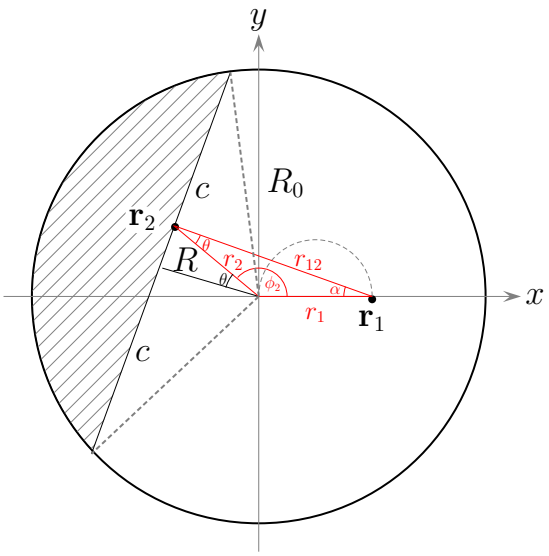

Figure 12: Choose a point $\mathbf{r}_2$ at random with $y \geq 0$ and $\pi/2 \leq \phi_2 \leq \pi$, that is, in the second quadrant. The hatched segment is defined by the chord that passes through the point $\mathbf{r}_2$ that is perpendicular to the vector $\mathbf{r}_{12} = \mathbf{r}_2 - \mathbf{r}_1$. If $\mathbf{r}_3$ falls within the hatched segment, then $\mathbf{r}_{12} \cdot \mathbf{r}_{23} > 0$ and the movement is forward. Geometry reveals that $r_2 = r_{12}\cos\theta - r_1\cos(\pi - \phi_2) = r_{12}\cos\theta + r_1\cos\phi_2$.

that is,

$$\cos\theta = \begin{cases} \frac{r_2 - r_1\cos\phi_2}{r_{12}}, \\ \frac{-r_2 + r_1\cos\phi_2}{r_{12}}, \\ \frac{r_2 - r_1\cos\phi_2}{r_{12}}. \end{cases} \tag{40}$$

Finally, we need to find r_{12}. Consider the red triangle with sides r_1, r_2 and r_{12}. Because the Law of Cosines is generic, then in all three cases

$$r_{12}^2 = r_1^2 + r_2^2 - 2r_1 r_2\cos\phi_2. \tag{41}$$

Now, combining Eq.(38), Eq.(40), and Eq.(41) we find

$$R\left(r_1, r_2, \phi_2\right) = \begin{cases} \frac{r_2^2 - r_1 r_2\cos\phi_2}{\sqrt{r_1^2 + r_2^2 - 2r_1 r_2\cos\phi_2}}, \\ \frac{-r_2^2 + r_1 r_2\cos\phi_2}{\sqrt{r_1^2 + r_2^2 - 2r_1 r_2\cos\phi_2}}, \\ \frac{r_2^2 - r_1 r_2\cos\phi_2}{\sqrt{r_1^2 + r_2^2 - 2r_1 r_2\cos\phi_2}}. \end{cases} \tag{42}$$

The probability density for choosing a point with radius r is

$$P(r)dr = \frac{2r}{R_0^2}dr, \tag{43a}$$

such that

$$\int_0^{R_0} P(r)dr = \int_0^{R_0} \frac{2r}{R_0^2}dr = \left[\frac{r^2}{R_0^2}\right]_0^{R_0} = 1. \tag{43b}$$

The probability density for choosing a point with angle ϕ_2 is

$$P(\phi_2)d\phi_2 = \frac{1}{\pi}d\phi_2, \tag{44a}$$

such that

$$\int_0^{\pi} P(\phi_2)d\phi_2 = \left[\frac{1}{\pi}\phi_2\right]_0^{\pi} = 1. \tag{44b}$$

We recall that $R = R(r_1, r_2, \phi_2)$. The probability that the movement is forward when $\alpha = 1$ is

$$\begin{aligned}
p_{\bigcirc}(\alpha) &= \frac{\int_0^{R_0} \frac{2r_1}{R_0^2}dr_1 \int_0^{R_0} \frac{2r_2}{R_0^2}dr_2 \int_0^{\pi} \frac{1}{\pi}d\phi_2 A(R, R_0)}{\pi R_0^2} \\
&= \frac{4}{\pi^2 R_0^6}\int_0^{R_0} dr_1 \int_0^{R_0} dr_2 \int_0^{\pi} d\phi_2 r_1 r_2 A(R, R_0) \\
&= \frac{4}{\pi^2 R_0^6}\Bigg(\int_0^{R_0} dr_1 \int_0^{\pi/2} d\phi_2 \int_{r_1\cos\phi_2}^{R_0} dr_2 r_1 r_2 A(R, R_0) \\
&\qquad + \int_0^{R_0} dr_1 \int_0^{\pi/2} d\phi_2 \int_0^{r_1\cos\phi_2} dr_2 r_1 r_2 A^{+}(R, R_0) \\
&\qquad + \int_0^{R_0} dr_1 \int_{\pi/2}^{\pi} d\phi_2 \int_0^{R_0} dr_2 r_1 r_2 A(R, R_0)\Bigg),
\end{aligned} \tag{45}$$

where the distance R is given by Eq.(42) as a function of the radii r_1 and r_2 and the angle ϕ_2. Because of the symmetry $A^{+}(R, R_0) = A(-R, R_0)$, then combined with Eq.(42), the exact result can (miraculously) be written

$$p_{\bigcirc}(\alpha) = \frac{4}{\pi^2 R_0^6}\int_0^{R_0}\int_0^{R_0}\int_0^{\pi} r_1 r_2 A(R, R_0)\, dr_1 dr_2 d\phi_2, \tag{46a}$$

$$R(r_1, r_2, \phi_2) = \frac{r_2^2 - r_1 r_2\cos\phi_2}{\sqrt{r_1^2 + r_2^2 - 2r_1 r_2\cos\phi_2}}. \tag{46b}$$

We will now show that the probability of going forward is independent of the radius R_0 of the circle. We substitute the variables $u_1 = r_1/R_0$ and $u_2 = r_2/R_0$, implying that the

upper limits of the integrals involving r_1 and r_2 become 1:

$$p_{\bigcirc}(\alpha) = \frac{4}{\pi^2 R_0^6} \int_0^1 \int_0^1 \int_0^\pi u_1 u_2 R_0^2 A\left(R(u_1 R_0, u_2 R_0, \phi_2), R_0\right) R_0^2 du_1 du_2 d\phi_2. \tag{47}$$

We notice that

$$A\left(R(u_1 R_0, u_2 R_0, \phi_2), R_0\right) = A\left(R_0 R(u_1, u_2, \phi_2), R_0\right) = R_0^2 A(R, 1) \tag{48}$$

such that (after changing the dummy variables u_1, u_2 to r_1, r_2)

$$p_{\bigcirc}(\alpha) = \frac{4}{\pi^2} \int_0^1 \int_0^1 \int_0^\pi r_1 r_2 A\left(R, 1\right) dr_1 dr_2 d\phi_2, \tag{49a}$$

$$R\left(r_1, r_2, \phi_2\right) = \frac{r_2^2 - r_1 r_2 \cos\phi_2}{\sqrt{r_1^2 + r_2^2 - 2 r_1 r_2 \cos\phi_2}} \tag{49b}$$

which is independent on R_0.

Using numerical integration (and $\phi_2 = \phi$)

$dr = 1/nr$
$d\phi = \pi/n\phi$
int $= 0$
do $n_1 = 1, nr$
  $r_1 = (n_1 - \frac{1}{2})dr$
  do $n_2 = 1, nr$
    $r_2 = (n_2 - \frac{1}{2})dr$
    do $n_3 = 1, n\phi$
      $\phi = (n_3 - \frac{1}{2})d\phi$
      $R = \frac{r_2^2 - r_1 r_2 \cos\phi}{\sqrt{r_1^2 + r_2^2 - 2 r_1 r_2 \cos\phi}}$
      $A(R, 1) = \cos^{-1} R - R\sqrt{1 - R^2}$
      int $=$ int $+ r_1\, r_2\, A(R, 1)\, dr\, dr\, d\phi$
    end do
  end do
end do
$p_{\bigcirc}(\alpha) = \frac{4}{\pi^2}$ int

We start numerical integration with $nr = 8 \Leftrightarrow dr = 0.125$ and $n\phi = 26 \Leftrightarrow d\phi = 0.121$ such that the accuracy of dr and $d\phi$ is comparable. For each iteration, we double the precision. Because it is a 3-fold integral, the computing time the increases by a factor of about $2^3 = 8$ for each iteration:

nr	$n\phi$	$p_{\bigcirc}(\alpha = 1)$
8	26	0.240442613132
16	52	0.240036492588
32	104	0.239937628777
64	208	0.239913189587
128	416	0.239907109902
256	832	0.239905593384
512	1664	0.239905214650
1024	3328	0.239905120014
2048	6656	0.239905096361
4096	13312	0.239905090452
8192	26624	0.239905088607
16384	53248	0.239905088649

The cpu time (sequential, without any parallel computing) for the highest precision with $nr = 16384$ and $n\phi = 53248$ is about 9 days and we find

$$p_{\bigcirc}(\alpha = 1) = 0.23990508 \tag{50}$$

which is consistent with the Monte Carlo estimate, see Sec. 5.3.

C.2 General analytical method in $2D$

We have already seen in Section 3 that for simple geometries writing down an analytic expression for the probability of forward movement is generally straightforward. Difficulties arise when we attempt to render our numerical evaluations of such expressions more efficient by reducing the number and range of integration of the associated variables.

In 2D and in the specific case for $\alpha = 1$, a general method can be applied to reduce the basic 6-fold integral in Cartesian coordinates to a 3-fold integral in polar coordinates. The idea, inspired by the full range solution of the 1D problem presented in Appendix A.1.3, is to only integrate over the coordinates x_i, y_i of the central point of a triplet $\mathbf{r}_{i-1}, \mathbf{r}_i, \mathbf{r}_{i+1}$ and an angle variable ϕ determining a particular separation of the bounded space.

As for the 1D case, forward movement corresponds to $\mathbf{r}_{i-1}$ and $\mathbf{r}_{i+1}$ being on opposite sides of this separator. Note that $\mathbf{r}_{i-1}$ has to lay on the normal to the separator intersecting the latter at the central point $\mathbf{r}_i$. As a consequence of this, and unlike the $1D$ case, the two configurations corresponding to forward movement are not weighted equally. In particular, we have to introduce a measure of "how many" $\mathbf{r}_{i-1}$ are consistent with a particular choice of x, y, ϕ. An example is given in Fig. 13 for the case of a unit square.

The weight associated with a particular configuration has to be proportional to the infinitesimal area δA of bounded space swept by the normal to the separator as $\phi \to$

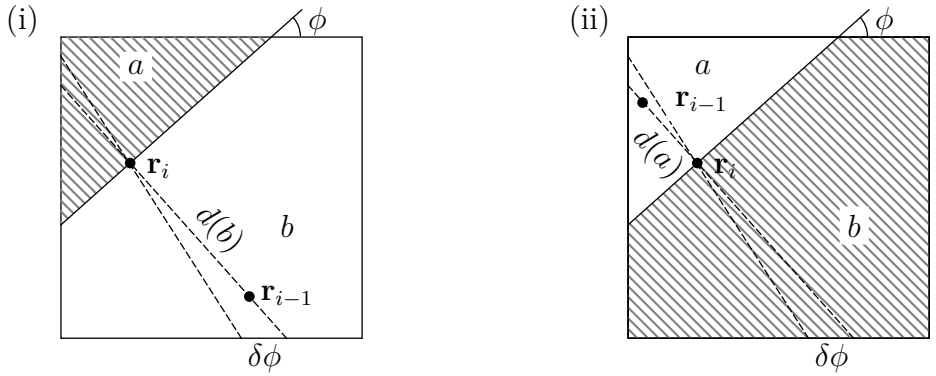

Figure 13: Two specular cases for the unit square. A separator passing though the central point of a triplet with an angle ϕ defines the forward movement region (hatched area). Previous stopping positions $\mathbf{r}_{i-1}$ consistent with this picture have to be found along the normal to the separator. An infinitesimal change in angle $\delta\phi$ is exaggerated for the sake of exposition.

$\phi + \delta\phi$, which is given in polar coordinates by

$$\delta A = \frac{1}{2} d^2 \delta\phi, \tag{51}$$

where $d = d(b)$ for case (i) and $d = d(a)$ for case (ii) in Fig. 13. A general expression for the 3-fold integral when $\alpha = 1$ could therefore be written as

$$p_{2\mathrm{D}}(\alpha) = \int\int\int_0^{\pi} \frac{(d^2(a) + d^2(b))\, ab}{2(a+b)^3}\, d\phi dy dx, \tag{52}$$

where $a = a(x, y, \phi)$, $b = b(x, y, \phi)$ and the inverse factors of $(a+b)$ ensure normalisation. The form of $d(a; x, y, \phi)$ is strongly geometric specific but can be found exactly for simple shapes. We have done this for the case of a unit square and unit circle, with numerical results reported in the tables below.

We start numerical integration with $nx = ny = 8 \Leftrightarrow dx = dy = 0.125$ and $n\phi = 50$. For each iteration, we double the precision. Because it is a 3-fold integral, the computing time increases by a factor of about $2^3 = 8$ for each iteration:

$nx = ny$	$n\phi$	$p_{\square}(\alpha = 1)$
8	50	0.242247390361
16	100	0.241852581074
32	200	0.241764067138
64	400	0.241742596821
128	800	0.241737262303
256	1600	0.241735935418
512	3200	0.241735604403
1024	6400	0.241735521838
2048	12800	0.241735501211
4096	25600	0.241735496054
8192	51200	0.241735494739

The cpu time for the highest precision with $nx = ny = 8192$ and $n\phi = 51200$ is about 2 days and we find

$$p_{\square}(\alpha = 1) = 0.2417354, \tag{53}$$

which is consistent with the Monte Carlo estimate, see Sec. 5.3. For the circle, we start numerical integration with $nR = 8 \Leftrightarrow dr = 0.125$ and $n\phi = 50$. For each iteration, we double the precision. Because it is a 2-fold integral, the computing time increases by a factor of about $2^2 = 4$ for each iteration:

nR	$n\phi$	$p_{\bigcirc}(\alpha = 1)$
8	50	0.241067149258
16	100	0.240189514753
32	200	0.239975516491
64	400	0.239922616788
128	800	0.239909461163
256	1600	0.239906180506
512	3200	0.239905361344
1024	6400	0.239905156682
2048	12800	0.239905105525
4096	25600	0.239905092746
8192	51200	0.239905089543
16384	102400	0.239905088744

The cpu time for the highest precision with $nR = 8192$, $n\phi = 51200$ is about 2 days and we find

$$p_{\bigcirc}(\alpha = 1) = 0.23990508, \tag{54}$$

which is consistent with the Monte Carlo estimate, see Sec. 5.3.

Symmetries of the geometry can now be exploited to reduce the ranges of integration.

For example, a C_5 rotational symmetry reduces the xy surface of integration by a factor 5. This is why for the unit circle integration over the radius R is sufficient, although we need to take extra care in weighting contributions correctly.

The general method presented above can be extended to the $\Delta\ell < L_{\max}$ case, in which it is the intersection of bounded space and maximum range for one between-stops displacement that is divided into forward and backward regions by the separator. Note, however, that in this case the contribution for the midpoint of the triplet needs to be weighted by the steady-state stopping position distributions, which is no longer uniform.

D Monte Carlo simulations

We consider $N \geq 2$ samples of a given geometry $\mathcal{R}$, for example a circle, and given $\alpha = \Delta\ell/L_{\max}$. For each sample $k = 1, \ldots, N$ we can estimate the probability of going forward $p^k_{\mathcal{R}}(\alpha)$ by considering each triplet $\mathbf{r}_j, \mathbf{r}_{j+1}, \mathbf{r}_{j+2}$ in a sequence of $M+2$ stopping points $\{\mathbf{r}_j\}_{j=1}^{M+2}$. The probability $p^k_{\mathcal{R}}(\alpha)$ is the fraction of forward moving points $\mathbf{r}_{j+2}, j = 1, \ldots, M$ determined by considering $(\mathbf{r}_{j+2} - \mathbf{r}_{j+1})$ relative to $(\mathbf{r}_{j+1} - \mathbf{r}_j)$ for each of the M triplets. Doing this for N samples allows us to calculate the sample average, $p_{\mathcal{R}}(\alpha)$, the sample standard deviation, σ, and hence the standard error of the sample average, s:

$$p_{\mathcal{R}}(\alpha) = \frac{1}{N}\sum_{k=1}^{N} p^k_{\mathcal{R}}(\alpha), \tag{55a}$$

$$\sigma^2 = \frac{1}{N-1}\sum_{k=1}^{N}\left(p^k_{\mathcal{R}}(\alpha)\right)^2 - \frac{1}{N(N-1)}\left(\sum_{k=1}^{N} p^k_{\mathcal{R}}(\alpha)\right)^2, \tag{55b}$$

$$s = \frac{\sigma}{\sqrt{N}}. \tag{55c}$$

The specific way of generating the sequence of positions required for the Monte Carlo method will depend on the chosen boundary conditions. A particularly simple case, in all dimensions, is that of $\alpha = 1$ with "no-go" boundary conditions, where each stopping positions is chosen uniformly at random within the bounded region. Other setups involving $\alpha < 1$ and/or different boundary conditions are generally less trivial, especially in $d > 1$. To highlight some of these difficulties and given the particular relevance of $d = 2$ in the context of movement ecology, we devote Appendices D.1 and D.2 to the further discussion of how different boundary conditions are implemented numerically for the case of circular and square geometries.

Leaving aside the details of the implementation, the general procedure followed to generate a sample sequence of M stopping points can be broken down into the following steps:

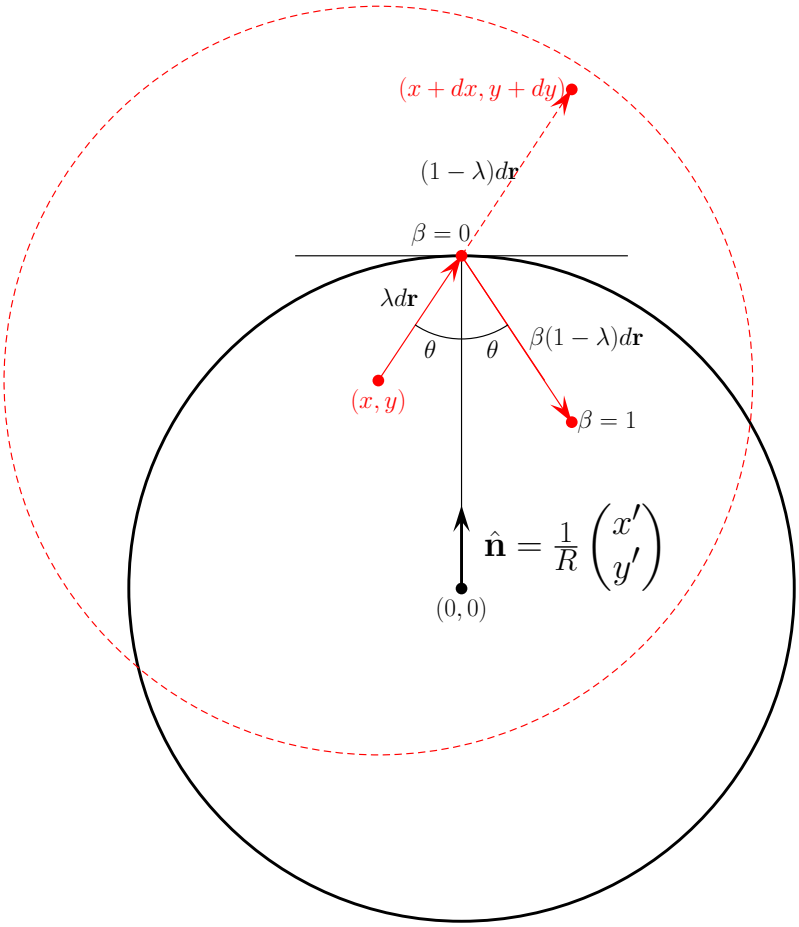

Figure 14: The bounded region is a circle with centre at $(x_0, y_0) = (0, 0)$ and radius R (black line). Let $\mathbf{r} = (x, y)$ denote a stopping point. The successive potential stopping point is chosen uniformly within a circle with centre at (x, y) and radius $\alpha 2R$ (red dashed line indicates $\alpha = 0.75$). The unit vector $\hat{\mathbf{n}}$ from the centre of the bounded region to the point at the periphery is used to find a general expression for the situation with "reflective" boundary condition.

1. Pick a random starting point within the bounded space $\mathcal{R}$ and append its coordinates to a list. With large M, the result would be independent on this initial choice.

2. Starting from the stopping point that was last appended to the list and consistently with the chosen boundary conditions, generate a new stopping point within the bounded space.

3. Append the coordinates of the point satisfying the above conditions to the list.

4. Return to Step 2. and repeat M times.

D.1 Circular Geometry in 2D

The bounded region is a circle with centre in $(0, 0)$ and radius R (indicated with black line in Fig. 14), so $L_{\max} = 2R$. Stopping point is $\mathbf{r} = (x, y)$. Next, choose a point uniformly within a circle centred at (x, y) with radius $\alpha L_{\max}$. In the sketch shown in Fig.

14, $\alpha = 0.75$. The new point is $\mathbf{r} + d\mathbf{r} = (x + dx, y + dy)$. If $(x + dx)^2 + (y + dy)^2 > R^2$, this point is *outside* the bounded region. Then we need to apply the appropriate boundary condition.

D.1.1 "No-go" boundary condition

For the "no-go" boundary condition, we discard the point and we choose another point uniformly distributed within the red-dashed circle until this point falls within the bounded region shown in black. This is then our new stopping position.

D.1.2 "Stop-go" boundary condition

For the "stop-go" boundary condition, the new stopping point is the intersection $\mathbf{r}' = (x', y')$ between the line from (x, y) to $(x + dx, y + dy)$ and the periphery of the circle $x^2 + y^2 = R^2$.

$$\begin{pmatrix} x' \\ y' \end{pmatrix} = \begin{pmatrix} x \\ y \end{pmatrix} + \lambda \begin{pmatrix} dx \\ dy \end{pmatrix} \Rightarrow (x + \lambda dx)^2 + (y + \lambda dy)^2 = R^2, \tag{56}$$

that is

$$(dx^2 + dy^2)\lambda^2 + (2xdx + 2ydy)\lambda + (x^2 + y^2 - R^2) = 0 \tag{57}$$

with (positive) solution

$$\lambda = \frac{-(2xdx + 2ydy) + \sqrt{(2xdx + 2ydy)^2 - 4(dx^2 + dy^2)(x^2 + y^2 - R^2)}}{2(dx^2 + dy^2)}. \tag{58}$$

Using this λ yields our new stopping position on the periphery $\mathbf{r}' = \mathbf{r} + \lambda d\mathbf{r}$.

D.1.3 "Reflective" boundary condition

The vector that is reflected from the boundary is the part of the vector from (x, y) to $(x + dx, y + dy)$ that is outside the bounded region, namely

$$\beta(1 - \lambda)d\mathbf{r} = \beta(1 - \lambda) \begin{pmatrix} dx \\ dy \end{pmatrix}, \tag{59}$$

where we have introduced the "damping" parameter β. As discussed in Appendix A.4, the limit $\beta = 1$ is associated with the perfectly elastic reflection while $\beta = 0$ is associated with a perfectly inelastic reflection, that is, the "stop-go" boundary condition.

To find a general expression for the reflection of this vector, let us denote the unit vector in the direction from the centre of the circle to the point at the periphery as

$$\hat{\mathbf{n}} = \frac{1}{\sqrt{x'^2 + y'^2}} \begin{pmatrix} x' \\ y' \end{pmatrix} = \frac{1}{R} \begin{pmatrix} x' \\ y' \end{pmatrix}, \tag{60}$$

as $x'^2 + y'^2 = R^2$ since (x', y') is a point on the periphery of the circle. We can use $\hat{\mathbf{n}}$ to find the projection of $\beta(1-\lambda)d\mathbf{r}$ along the direction on $\hat{\mathbf{n}}$ as $[\beta(1-\lambda)d\mathbf{r}\cdot\hat{\mathbf{n}}]\,\hat{\mathbf{n}}$ and the perpendicular component as $\beta(1-\lambda)d\mathbf{r} - [\beta(1-\lambda)d\mathbf{r}\cdot\hat{\mathbf{n}}]\,\hat{\mathbf{n}}$, so the vector from $\mathbf{r}'$ to the new stopping point within the region is

$$\beta(1-\lambda)d\mathbf{r} - 2\,[\beta(1-\lambda)d\mathbf{r}\cdot\hat{\mathbf{n}}]\,\hat{\mathbf{n}}, \tag{61}$$

implying that the new stopping point within the region is

$$\begin{aligned}\mathbf{r}' + \beta(1-\lambda)d\mathbf{r} - 2\,[\beta(1-\lambda)d\mathbf{r}\cdot\hat{\mathbf{n}}]\,\hat{\mathbf{n}} &= \mathbf{r} + \lambda d\mathbf{r} + \beta(1-\lambda)d\mathbf{r} - 2\,[\beta(1-\lambda)d\mathbf{r}\cdot\hat{\mathbf{n}}]\,\hat{\mathbf{n}} \\ &= \mathbf{r} + (\lambda+\beta-\beta\lambda)d\mathbf{r} - 2\,[\beta(1-\lambda)d\mathbf{r}\cdot\hat{\mathbf{n}}]\,\hat{\mathbf{n}}. \end{aligned}\tag{62}$$

We note that

$$\text{For } \beta = 1 \;:\; \mathbf{r} + d\mathbf{r} - 2\,[(1-\lambda)d\mathbf{r}\cdot\hat{\mathbf{n}}]\,\hat{\mathbf{n}}, \tag{63a}$$

$$\text{For } \beta = 0 \;:\; \mathbf{r} + \lambda d\mathbf{r}, \tag{63b}$$

which in coordinates read

$$\text{For } \beta = 1 \;:\; \begin{pmatrix} x + dx - 2(1-\lambda)(x'dx + y'dy)x'/R^2 \\ y + dy - 2(1-\lambda)(x'dx + y'dy)y'/R^2 \end{pmatrix}, \tag{64a}$$

$$\text{For } \beta = 0 \;:\; \begin{pmatrix} x' \\ y' \end{pmatrix} = \begin{pmatrix} x + \lambda dx \\ y + \lambda dy \end{pmatrix}. \tag{64b}$$

Note that multiple reflections might occur. Hence, when implementing the above, one has to use recursive programming for $\beta = 1$ as the reflection itself might be outside the bounded region.

D.2 Square Geometry in 2D

The bounded region is a square with centre in $(0, 0)$ and sides L (indicated with black line in Fig. 15), so $L_{\max} = \sqrt{2}L$. Stopping point is $\mathbf{r} = (x, y)$. Next, choose a point uniformly within a circle centred at (x, y) with radius $\alpha L_{\max}$. In the sketch shown in Fig. 15, $\alpha = 1.0$. The new point is $\mathbf{r} + d\mathbf{r} = (x + dx, y + dy)$. If $|x + dx| > L/2$ or $|y + dy| > L/2$, this point is *outside* the bounded region. Then we need to apply the appropriate boundary condition.

D.2.1 "No-go" boundary condition

For the "no-go" boundary condition, we discard the point $(x + dx, y + dy)$ and we choose another point uniformly distributed within the red-dashed circle until this point falls within the bounded region shown in black. This is then our new stopping position.

D.2.2 "Stop-go" boundary condition

For the "stop-go" boundary condition, the new stopping point is the intersection $\mathbf{r}' = (x', y')$ between the line from (x, y) to $(x + dx, y + dy)$ and the boundary of the square:

$$\begin{pmatrix} x' \\ y' \end{pmatrix} = \begin{pmatrix} x \\ y \end{pmatrix} + \lambda \begin{pmatrix} dx \\ dy \end{pmatrix}. \tag{65}$$

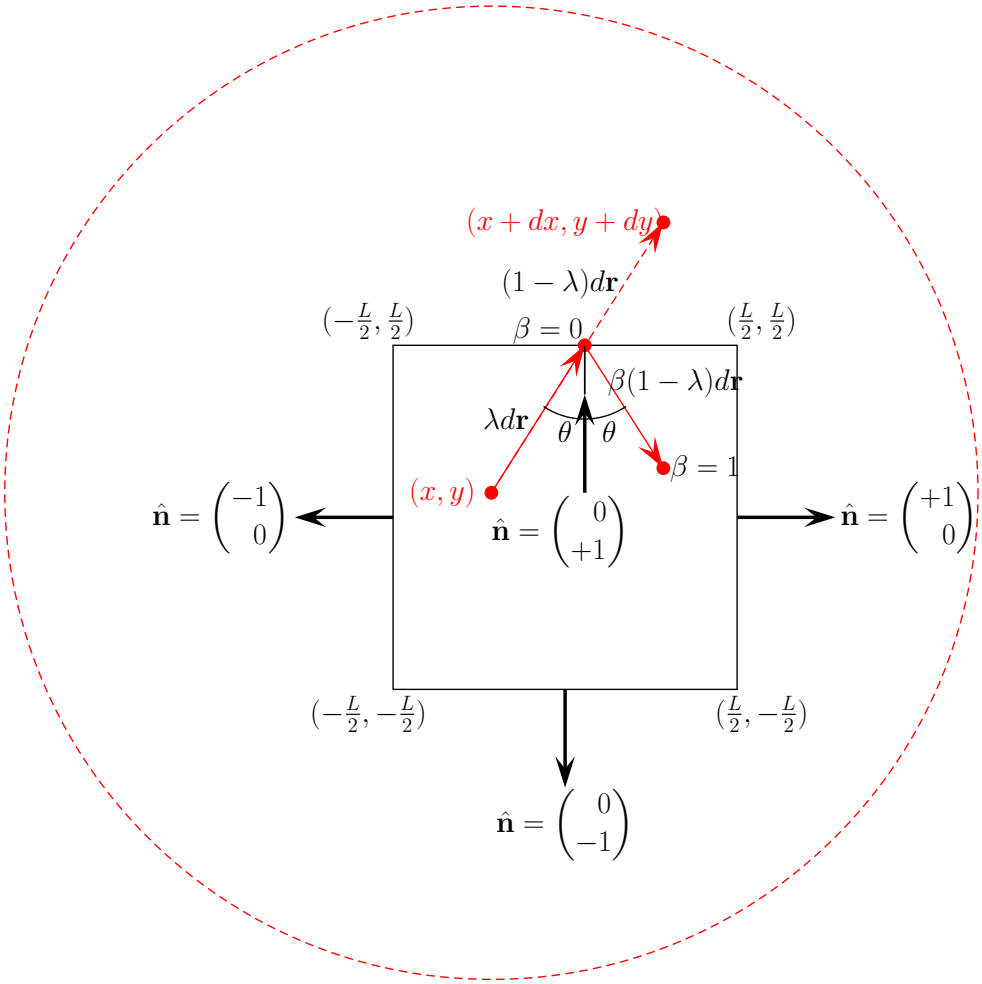

Figure 15: The bounded region is a square with centre at $(x_0, y_0) = (0, 0)$ and sides L (black line). Let $\mathbf{r} = (x, y)$ denote a stopping point. The successive potential stopping point is chosen uniformly within a circle with centre at (x, y) and radius $\alpha L_{\max}$ (red dashed line indicates $\alpha = 1$) where $L_{\max} = \sqrt{2}L$. The unit vector $\hat{\mathbf{n}}$ to a point at the boundary is used to find a general expression for the situation with "reflective" boundary condition.

We need to consider four different cases separately in order to uniquely determine on which of the four boundaries (x', y') is positioned. Recall that the stopping point within the region is (x, y). Assume $(x + dx, y + dy)$ is outside the bounded region. If

- $dx < 0, dy < 0$:

  (a) $\frac{dy}{dx} > \frac{-\frac{L}{2}-y}{-\frac{L}{2}-x} \Leftrightarrow y' = -\frac{L}{2} \Leftrightarrow \lambda = \frac{-\frac{L}{2}-y}{dy}$

  (b) $\frac{dy}{dx} < \frac{-\frac{L}{2}-y}{-\frac{L}{2}-x} \Leftrightarrow x' = -\frac{L}{2} \Leftrightarrow \lambda = \frac{-\frac{L}{2}-x}{dx}$

- $dx < 0, dy > 0$:

  (a) $\frac{dy}{dx} > \frac{\frac{L}{2}-y}{-\frac{L}{2}-x} \Leftrightarrow x' = -\frac{L}{2} \Leftrightarrow \lambda = \frac{-\frac{L}{2}-x}{dx}$

  (b) $\frac{dy}{dx} < \frac{\frac{L}{2}-y}{-\frac{L}{2}-x} \Leftrightarrow y' = \frac{L}{2} \Leftrightarrow \lambda = \frac{\frac{L}{2}-y}{dy}$

- $dx > 0, dy > 0$:

  (a) $\frac{dy}{dx} > \frac{\frac{L}{2}-y}{\frac{L}{2}-x} \Leftrightarrow y' = \frac{L}{2} \Leftrightarrow \lambda = \frac{\frac{L}{2}-y}{dy}$

  (b) $\frac{dy}{dx} < \frac{\frac{L}{2}-y}{\frac{L}{2}-x} \Leftrightarrow x' = \frac{L}{2} \Leftrightarrow \lambda = \frac{\frac{L}{2}-x}{dx}$

- $dx > 0, dy < 0$:

  (a) $\frac{dy}{dx} > \frac{-\frac{L}{2}-y}{\frac{L}{2}-x} \Leftrightarrow x' = \frac{L}{2} \Leftrightarrow \lambda = \frac{\frac{L}{2}-x}{dx}$

  (b) $\frac{dy}{dx} < \frac{-\frac{L}{2}-y}{\frac{L}{2}-x} \Leftrightarrow y' = -\frac{L}{2} \Leftrightarrow \lambda = \frac{-\frac{L}{2}-y}{dy}$

Using the relevant λ yields our new stopping position on the boundary $\mathbf{r}' = \mathbf{r} + \lambda d\mathbf{r}$. Note that we have disregarded the special cases of $dx = 0$ or $dy = 0$.

D.2.3 "Reflective" boundary condition

The vector that is reflected from the boundary is the part of the vector from (x, y) to $(x + dx, y + dy)$ that is outside the bounded region, namely

$$\beta(1 - \lambda)d\mathbf{r} = \beta(1 - \lambda)\begin{pmatrix} dx \\ dy \end{pmatrix}, \tag{66}$$

where we have introduced the parameter β. The limit $\beta = 1$ is associated with the perfectly elastic reflection while $\beta = 0$ is associated with a perfectly inelastic reflection,

that is, the "stop-go" boundary condition.

To find a general expression for the reflection of this vector, we note that we have four potential unit vectors perpendicular to the boundary of the square, namely

$$\hat{\mathbf{n}} = \begin{cases} \begin{pmatrix} 0 \\ +1 \end{pmatrix} & \text{associated with } y' = \frac{L}{2}, \\ \begin{pmatrix} +1 \\ 0 \end{pmatrix} & \text{associated with } x' = \frac{L}{2}, \\ \begin{pmatrix} 0 \\ -1 \end{pmatrix} & \text{associated with } y' = -\frac{L}{2}, \\ \begin{pmatrix} -1 \\ 0 \end{pmatrix} & \text{associated with } x' = -\frac{L}{2}. \end{cases} \tag{67}$$

We can use the relevant $\hat{\mathbf{n}}$ to find the projection of $\beta(1-\lambda)d\mathbf{r}$ along the direction on $\hat{\mathbf{n}}$ as $[\beta(1-\lambda)d\mathbf{r}\cdot\hat{\mathbf{n}}]\,\hat{\mathbf{n}}$ and the perpendicular component as $\beta(1-\lambda)d\mathbf{r} - [\beta(1-\lambda)d\mathbf{r}\cdot\hat{\mathbf{n}}]\,\hat{\mathbf{n}}$, so the vector from $\mathbf{r}'$ to the new stopping point within the region is

$$\beta(1-\lambda)d\mathbf{r} - 2\,[\beta(1-\lambda)d\mathbf{r}\cdot\hat{\mathbf{n}}]\,\hat{\mathbf{n}} \tag{68}$$

implying that the new stopping point within the region is

$$\begin{aligned} \mathbf{r}' + \beta(1-\lambda)d\mathbf{r} - 2\,[\beta(1-\lambda)d\mathbf{r}\cdot\hat{\mathbf{n}}]\,\hat{\mathbf{n}} &= \mathbf{r} + \lambda d\mathbf{r} + \beta(1-\lambda)d\mathbf{r} - 2\,[\beta(1-\lambda)d\mathbf{r}\cdot\hat{\mathbf{n}}]\,\hat{\mathbf{n}} \\ &= \mathbf{r} + (\lambda+\beta-\beta\lambda)d\mathbf{r} - 2\,[\beta(1-\lambda)d\mathbf{r}\cdot\hat{\mathbf{n}}]\,\hat{\mathbf{n}}. \end{aligned} \tag{69}$$

We note that

$$\text{For } \beta = 1 \quad : \quad \mathbf{r} + d\mathbf{r} - 2\,[(1-\lambda)d\mathbf{r}\cdot\hat{\mathbf{n}}]\,\hat{\mathbf{n}}, \tag{70a}$$

$$\text{For } \beta = 0 \quad : \quad \mathbf{r} + \lambda d\mathbf{r}. \tag{70b}$$

There is no general expression for λ and $\hat{\mathbf{n}}$ as in the simpler case of the circle. Hence, we need to consider the eight cases separately in order to convert the above equations into coordinates.

For $\beta = 0$, the new stopping point on the boundary has coordinates

$$\begin{pmatrix} x' \\ y' \end{pmatrix} = \begin{pmatrix} x + \lambda dx \\ y + \lambda dy \end{pmatrix}, \tag{71}$$

using the appropriate expression for λ associated with each of the eight different cases.

For $\beta = 1$, the coordinates of the new stopping point after reflection is

- $dx < 0, dy < 0$:

  (a) $\frac{dy}{dx} > \frac{-\frac{L}{2}-y}{-\frac{L}{2}-x} \Leftrightarrow y' = -\frac{L}{2} \Leftrightarrow \lambda = \frac{-\frac{L}{2}-y}{dy}$; $\hat{\mathbf{n}} = \begin{pmatrix} 0 \\ -1 \end{pmatrix}$; $(d\mathbf{r} \cdot \hat{\mathbf{n}})\hat{\mathbf{n}} = \begin{pmatrix} 0 \\ dy \end{pmatrix}$
  $\begin{pmatrix} x + dx \\ y + dy - 2(1-\lambda)dy \end{pmatrix}$

  (b) $\frac{dy}{dx} < \frac{-\frac{L}{2}-y}{-\frac{L}{2}-x} \Leftrightarrow x' = -\frac{L}{2} \Leftrightarrow \lambda = \frac{-\frac{L}{2}-x}{dx}$; $\hat{\mathbf{n}} = \begin{pmatrix} -1 \\ 0 \end{pmatrix}$; $(d\mathbf{r} \cdot \hat{\mathbf{n}})\hat{\mathbf{n}} = \begin{pmatrix} dx \\ 0 \end{pmatrix}$
  $\begin{pmatrix} x + dx - 2(1-\lambda)dx \\ y + dy \end{pmatrix}$

- $dx < 0, dy > 0$:

  (a) $\frac{dy}{dx} > \frac{\frac{L}{2}-y}{-\frac{L}{2}-x} \Leftrightarrow x' = -\frac{L}{2} \Leftrightarrow \lambda = \frac{-\frac{L}{2}-x}{dx}$; $\hat{\mathbf{n}} = \begin{pmatrix} -1 \\ 0 \end{pmatrix}$; $(d\mathbf{r} \cdot \hat{\mathbf{n}})\hat{\mathbf{n}} = \begin{pmatrix} dx \\ 0 \end{pmatrix}$
  $\begin{pmatrix} x + dx - 2(1-\lambda)dx \\ y + dy \end{pmatrix}$

  (b) $\frac{dy}{dx} < \frac{\frac{L}{2}-y}{-\frac{L}{2}-x} \Leftrightarrow y' = \frac{L}{2} \Leftrightarrow \lambda = \frac{\frac{L}{2}-y}{dy}$; $\hat{\mathbf{n}} = \begin{pmatrix} 0 \\ +1 \end{pmatrix}$; $(d\mathbf{r} \cdot \hat{\mathbf{n}})\hat{\mathbf{n}} = \begin{pmatrix} 0 \\ dy \end{pmatrix}$
  $\begin{pmatrix} x + dx \\ y + dy - 2(1-\lambda)dy \end{pmatrix}$

- $dx > 0, dy > 0$:

  (a) $\frac{dy}{dx} > \frac{\frac{L}{2}-y}{\frac{L}{2}-x} \Leftrightarrow y' = \frac{L}{2} \Leftrightarrow \lambda = \frac{\frac{L}{2}-y}{dy}$; $\hat{\mathbf{n}} = \begin{pmatrix} 0 \\ +1 \end{pmatrix}$; $(d\mathbf{r} \cdot \hat{\mathbf{n}})\hat{\mathbf{n}} = \begin{pmatrix} 0 \\ dy \end{pmatrix}$
  $\begin{pmatrix} x + dx \\ y + dy - 2(1-\lambda)dy \end{pmatrix}$

  (b) $\frac{dy}{dx} < \frac{\frac{L}{2}-y}{\frac{L}{2}-x} \Leftrightarrow x' = \frac{L}{2} \Leftrightarrow \lambda = \frac{\frac{L}{2}-x}{dx}$; $\hat{\mathbf{n}} = \begin{pmatrix} +1 \\ 0 \end{pmatrix}$; $(d\mathbf{r} \cdot \hat{\mathbf{n}})\hat{\mathbf{n}} = \begin{pmatrix} dx \\ 0 \end{pmatrix}$
  $\begin{pmatrix} x + dx - 2(1-\lambda)dx \\ y + dy \end{pmatrix}$

- $dx > 0, dy < 0$:

  (a) $\frac{dy}{dx} > \frac{-\frac{L}{2}-y}{\frac{L}{2}-x} \Leftrightarrow x' = \frac{L}{2} \Leftrightarrow \lambda = \frac{\frac{L}{2}-x}{dx}$; $\hat{\mathbf{n}} = \begin{pmatrix} +1 \\ 0 \end{pmatrix}$; $(d\mathbf{r} \cdot \hat{\mathbf{n}})\hat{\mathbf{n}} = \begin{pmatrix} dx \\ 0 \end{pmatrix}$
  $\begin{pmatrix} x + dx - 2(1-\lambda)dx \\ y + dy \end{pmatrix}$

(b) $\frac{dy}{dx} < \frac{-\frac{L}{2}-y}{\frac{L}{2}-x} \Leftrightarrow y' = -\frac{L}{2} \Leftrightarrow \lambda = \frac{-\frac{L}{2}-y}{dy}$; $\hat{\mathbf{n}} = \begin{pmatrix} 0 \\ -1 \end{pmatrix}$; $(d\mathbf{r} \cdot \hat{\mathbf{n}})\hat{\mathbf{n}} = \begin{pmatrix} 0 \\ dy \end{pmatrix}$

$$\begin{pmatrix} x + dx \\ y + dy - 2(1-\lambda)dy \end{pmatrix}$$

Note that multiple reflections might occur. Hence, when implementing the above, one has to use recursive programming for $\beta = 1$ as the reflection itself might be outside the bounded region.

D.3 Numerical results for circular and square geometries in 2D

The analytic result for the circle for "no-go" boundary condition demonstrated explicitly that the probability of forward movement between stopping points is independent of the linear dimension (diameter) of the circle, see C.1. This result is true for all boundary conditions and all geometries. Figure 16 shows the probability of moving forward in circular and square geometries in 2D as a function of the diameter and diagonal, respectively. Each of the tree boundary conditions "no-go", "stop-go" and "reflective", the probability of forward movement is invariant for a given geometry.

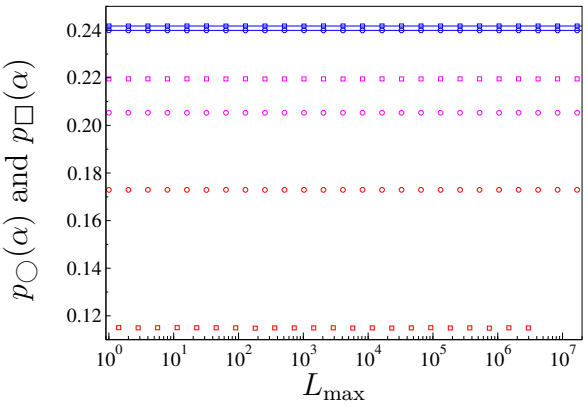

Figure 16: The probability of moving forward $p_{\bigcirc}(\alpha)$ and $p_{\square}(\alpha)$ versus the diameter of a circle and the diagonal of a squares $L_{\max}$ for $\alpha = \Delta\ell/L_{\max} = 1$ for various boundary conditions. The number of samples for each data point $N = 10000$, each with a sequence of $M = 10^5$ stopping points. The error bars (two standard deviations) are less than the symbol sizes. The geometry is indicated with the symbol (circle or square, respectively) while the color-coding yields the associated boundary condition of "no-go" (blue), "stop-go" (red) and "reflective" (magenta), respectively. The two blue lines are the analytical results $p_{\bigcirc}(\alpha) = 0.2399050$ and $p_{\square}(\alpha) = 0.2417354$ for the "no-go" boundary condition.

Figure 17 shows the probability of moving forward in circular and square geometries in 2D as a function of the dimensionless ratio $\alpha = \Delta\ell/L_{\max}$ for the tree boundary conditions "no-go", "stop-go" and "reflective". For all boundary conditions, there is a crossover from

a forward probability < 0.25 when $\alpha = 1$ to $1/2$ (indicated with the horizontal black line) when decreasing α from 1 to 0.

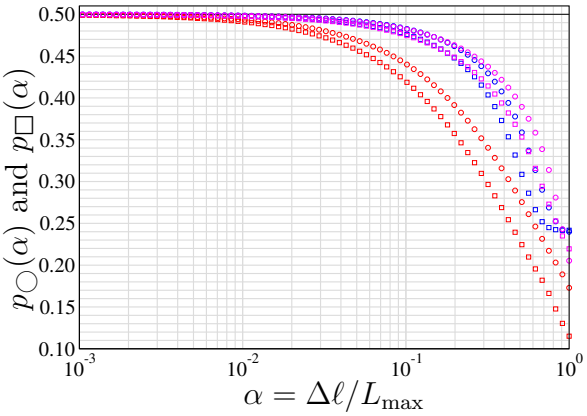

Figure 17: Numerical results for the probability of moving forward $p_{\bigcirc}(\alpha)$ and $p_{\square}(\alpha)$ in a circle or square versus the dimensionless ratio $\alpha = \Delta\ell/L_{\max}$ where $\Delta\ell$ is the maximum displacement between stopping positions for various boundary conditions. The number of samples for each data point $N = 10000$, each with a sequence of $M = 10^5$ stopping points. The error bars (two standard deviations) are less than the symbol sizes. The geometry is indicated with the symbol (circle or square, respectively) while the color-coding yields the associated boundary condition of "no-go" (blue), "stop-go" (red) and "reflective" (magenta), respectively.

E Step-by-step procedure for hypothesis testing

1. Classify each position along the trajectory of the studied individual as a "stop" or a "go". For two different definitions of a "stop" see [13, 14]. The total number of stopping positions is $M + 2$ where M is the number of successive pairs of stops.

2. Determine whether the absolute value of the smallest angle between the displacement vectors for successive stops, θ, is less than 90° or greater than or equal to 90° using the dot-product method (Appendix B).

3. Classify each movement between successive stops as forward or backward using the definition of forward movement as $\theta < 90°$ (Fig. 4, Subsection 5.1).

4. Calculate the empirical probability, $\hat{p}$, of the studied individual to move forward between stopping positions by dividing the number of forward moves by the total number of moves between stops, M.

5. Calculate the 95% Confidence Interval for the empirical probability of moving for-

ward as $\hat{p} \pm 1.96\sqrt{\frac{\hat{p}(1-\hat{p})}{M}}$.

6. Calculate the aspect ratio $0 \leq r \leq 1$ between the smallest and largest side for a rectangle or between the minor and major axis for an ellipse. An aspect ratio $r = 1$ would represent a square or a circle, respectively. Round the value of r to the second decimal place. For example, if $r = 0.754$, round it to 0.75.

7. Calculate $L_{\max}$ for the experimental arena or study area. If it has a rectangular shape, $L_{\max}$ is measured by the diagonal and if it has an elliptical shape, $L_{\max}$ is the length the major axis.

8. Calculate $\Delta\ell$ from the data. For example, this could be the larger of the following two values: (a) the maximum distance between successive stops or (b) the maximum distance between a stop and the most distant point along the path of the subsequent move.

9. Calculate the ratio $\alpha = \Delta\ell/L_{\max}$. Round the value of α to the second decimal place. For example, if $\alpha = 0.807$, round it to 0.81.

10. Open the file "TableS1.pdf" or "TableS2.pdf" for the tabulated expected probabilities of moving forward for a rectangle or an ellipse, respectively, under the "no-go" boundary condition. The values of α are given with precision to the second decimal place, beginning at 1.00 and ending at 0.01. For each value of α, there are 100 values of the aspect ratio r with precision to the second decimal place beginning with 1.00 and ending with 0.01.

11. Search for the value corresponding to the calculated α rounded to the second decimal place, 0.81, for example. To do this write "alpha = 0.81" in the box for the menu 'Edit '→ 'Find '.

12. Once the required value of α has been found, look down the column for p forward against the line for the appropriate aspect ratio, 0.75, for example.

13. Read the value for the appropriate probability of moving forward under the column p forward. For example, for $\alpha = 0.81$ and an aspect ratio $r = 0.75$, the probability of moving forward is $p = 0.2479$ for a rectangle (Table S1) and $p = 0.2470$ for an ellipse (Table S2).

14. Similarly, for $\alpha = 0.13$ and an aspect ratio $r = 0.15$, the probability of moving forward is $p = 0.3977$ for a rectangle (Table S1) and $p = 0.3951$ for an ellipse (Table S2).

15. Compare the 95% confidence interval for the empirical probability of moving forward with the expected probability read from Table S1 or S2. If the expected probability is outside the 95% confidence interval for the empirical probability, there is only 5% chance that the movement between stops lacks directional persistence. This means the probability that the null hypothesis is true is small. Therefore, it could be concluded that there is some evidence for the alternative hypothesis, namely that directional persistence is involved in the movement between stops.